Structural evolution of the Yushu-Nangqian region and its relationship to syncollisional igneous activity, east-central Tibet

Matthew S. Spurlin[†]
An Yin[‡]
Department of Earth and Space Sciences, and Institute of Geophysics and Planetary Physics, University of California, Los Angeles, California 90095-1567, USA

Brian K. Horton
Department of Earth and Space Sciences, University of California, Los Angeles, California 90095-1567, USA

Jiangyu Zhou
Jianghai Wang
Guangzhou Institute of Geochemistry, Chinese Academy of Sciences, Guangzhou, People's Republic of China

ABSTRACT

Field mapping, geochronological analyses, and cross section construction reveal a protracted deformation history and a minimum of 61 km of Cenozoic NE-SW shortening (in present coordinates) across the Yushu-Nangqian thrust belt in northern Tibet. Cenozoic contraction started prior to 51 Ma and was followed first by northwest-striking right-slip faulting and later by northwest-striking left-slip faulting. Renewed NE-SW contraction is expressed by folding of Neogene strata and thrusting, which again was followed by northwest-striking left-slip faults. Late Neogene deformation is expressed by local north-striking normal faults. Shortening across the Yushu-Nangqian belt appears to be accommodated by thin-skinned thrusting, which raises the question of how the deformation was accommodated in the lower crustal levels. To resolve this problem, we perform geochemical analysis of igneous rocks dated as 51–49 and 38–37 Ma. The rocks exhibit geochemical signatures characteristic of subduction, which implies that coeval crustal thickening in northeastern Tibet was most likely induced by continental subduction.

Keywords: Asia, China, Tibetan Plateau, thrust belts, strike-slip faults, syncollisional magmatism.

INTRODUCTION

The formation of the Tibetan Plateau has been attributed to continent-continent collision since ca. 70–50 Ma (e.g., Dewey and Burke, 1973; Molnar and Tapponnier, 1975; Patriat and Achache, 1984; Besse et al., 1984; Dewey et al., 1988, 1989; Le Pichon et al., 1992; Klootwijk et al., 1992, 1994; Beck et al., 1995; Rowley, 1996; Yin and Harrison, 2000; Tapponnier et al., 2001; DeCelles et al., 2002). Because of the important implications for continental dynamics and global climate change, mechanisms for Tibetan uplift and growth have been hotly debated. Models emphasizing the role of contraction during Cenozoic Indo-Asian collision include: (1) distributed crustal shortening (Dewey and Burke, 1973) or vertically uniform contraction of the Tibetan lithosphere (England and Houseman, 1986; Dewey et al., 1988), (2) northward underthrusting of either the whole Indian crust (Argand, 1924; Powell and Conaghan, 1973; Ni and Barazangi, 1984) or only its lower portion (Owens and Zandt, 1997; DeCelles et al., 2002), with possible assistance from southward underthrusting of Asia (Powell and Conaghan, 1973; Willett and Beaumont, 1994) or intraplateau continental subduction (Meyer et al., 1998; Yin and Harrison, 2000; Wang et al., 2001), (3) injection of the Indian continent into Tibetan ductile lower crust (Zhao and Morgan, 1987; Royden, 1996; Royden et al., 1997; Beaumont et al., 2001), and (4) distributed crustal shortening coupled with discrete left-slip faulting and subduction of continental mantle lithosphere (Mattauer, 1986; Meyer et al., 1998; Roger et al., 2000; Tapponnier et al., 2001). The thermal effect in the mantle for Tibetan uplift has also been considered. Specifically, convective removal of Tibetan mantle lithosphere may have raised the plateau over a couple of million years from an elevation of 3.5–4 km to its current and possibly maximum elevation of ~5 km (England and Houseman, 1989; Harrison et al., 1992; Molnar et al., 1993). In contrast to the Cenozoic models, the role of Mesozoic crustal shortening, either due to construction of an Andean-type margin (England and Searle, 1986) or pre-Cenozoic collision (Arne et al., 1997; Murphy et al., 1997; Worley et al., 1997; Hildebrand et al., 2001), has also been emphasized.

Growth of the Tibetan Plateau has long been considered to propagate northward (e.g., Burchfiel and Royden, 1991; Meyer et al., 1998). But this conclusion is mainly based on studies in the northernmost part of the plateau and has not been tested for the central and southern plateau. Related to this issue is whether syncollisional igneous activity in the plateau was related to continental subduction (Deng, 1989; Tapponnier et al., 1990, 2001; Meyer et al., 1998; Roger et al., 2000; Wang et al., 2001), convective removal of mantle lithosphere (England and Houseman, 1989; Molnar et al., 1993), or rollback of the subducted Indian slab (DeCelles et al., 2002; Ding et al., 2003). The continental-subduction model predicts coeval syncollisional igneous activity and crustal shortening, the convective-removal model predicts coeval igneous activity and extension, and finally, the slab rollback model predicts southward younging of igneous activity. The distinctions of the models require that field tests be conducted in regions where temporal relationships between Cenozoic deformation and igneous activities can be established. The Fenghuo Shan–Nangqian thrust belt in central Tibet (Fig. 1) is ideal because

[†]E-mail: mspurlin@bbl-inc.com.
[‡]E-mail: yin@ess.ucla.edu.

GSA Bulletin; September/October 2005; v. 117; no. 9/10; p. 1293–1317; doi: 10.1130/B25572.1; 15 figures; 4 tables; Data Repository item 2005149.

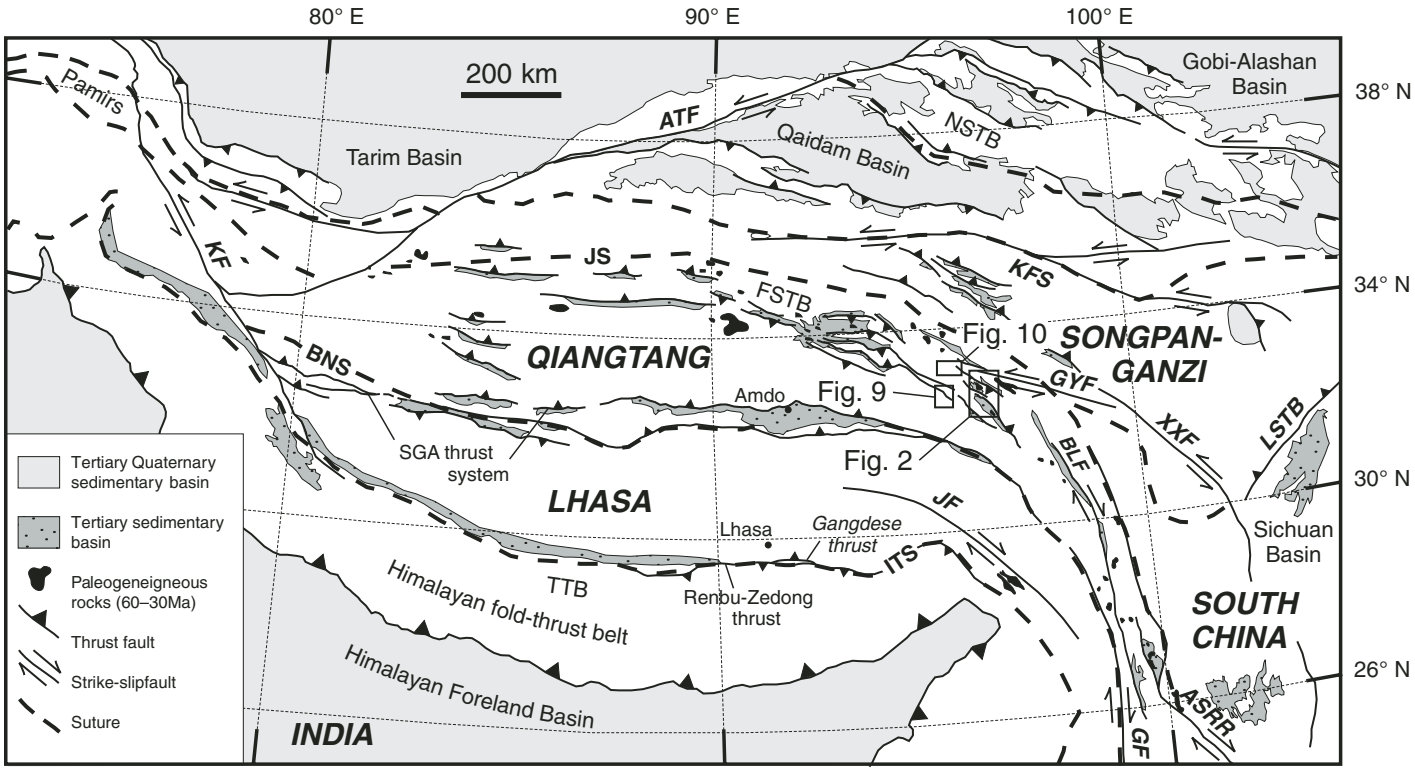

Figure 1. Simplified tectonic map of the Tibetan Plateau. Shown are sutures (JS—Jinsha suture; BNS—Banggong-Nujiang suture; ITS—Indus Tsangpo suture), major faults (KF—Karakorum fault; ATF—Altyn Tagh fault; KFS—Kunlun fault system; GYF—Ganzi-Yushu fault; XXF—Xianshuihe-Xiaojiang fault system; LSTB—Longmen Shan thrust belt; ASRR—Ailao Shan–Red River shear zone; GF—Gaoligong fault; JF—Jiali fault: BLF—Batang-Lijiang fault system), general locations of the five major Cenozoic thrust belts within the Himalaya-Tibet orogen (TTB—Tethyan thrust belt; Gangdese and Renbu-Zedong thrusts; SGA—Shiquanhe-Gaize-Amdo thrust system; FSTB—Fenghuo Shan thrust belt; NSTB—Nan Shan thrust belt), Tertiary-Quaternary sedimentary basins within and along the periphery of the Tibetan Plateau, and the distribution of Paleogene igneous rocks in northern Tibet (modified from Yin and Harrison, 2000).

it preserves both syncollisional structures and igneous rocks (Coward et al., 1988; Leeder et al., 1988; Pan et al., 1990; Zhang and Zheng, 1994; Yin and Nie, 1996; Chung et al., 1998; Yin and Harrison, 2000; Liu and Wang, 2001; Horton et al., 2002; Liu et al., 2003). Below we report our new field observations from this thrust belt in three areas: the Yushu-Nangqian traverse, the Dongba area, and the Zhaduo area (Fig. 1). Results of our geochronological and geochemical analyses are also documented.

GEOLOGY OF THE YUSHU-NANGQIAN AREA

An ~115-km-long, north-south traverse was mapped between Yushu and Nangqian (Fig. 2).[1] The area is bounded to the north by the active left-slip Ganzi-Yushu fault (Allen et al., 1984; Wang and Burchfiel, 2000) and to the south by the Cenozoic Nangqian basin (Fig. 2). North of the Ganzi-Yushu fault lie Triassic strata locally overlain by Tertiary sediments that are possibly bounded by thrusts as the northern extension of the Yushu-Nangqian thrust belt (Qinghai BGMR, 1991; Fig. 2). The Ganzi-Yushu fault is an en echelon left step-over of the ~1400-km-long Xianshuihe-Xiaojiang fault system in eastern Tibet (Fig. 1) (Ding, 1984; Allen et al., 1991; Wang et al., 1998; Wang and Burchfiel, 2000; Xu and Kamp, 2000), which has a total left slip of 78–100 km and may have been active for at least the past 4 m.y. (Wang and Burchfiel, 2000).

Stratigraphy

Major stratigraphic units exposed along the Yushu-Nangqian traverse are Carboniferous-Triassic marine carbonates and minor clastic units overlain by Jurassic, Cretaceous, and Paleogene red beds (Liu, 1988; Qinghai BGMR, 1991) (Fig. 2). The southern map area consists mostly of the Carboniferous Zhaduo Group (C_1zd), whereas the northern map area is dominated by the younger Upper Triassic Jieza Group (T_3jz). Triassic strata decrease in thickness from ~4400 m in the Nangqian area in the south to ~3200 m in the Shanglaxiu area in the north (Fig. 2) (Qinghai BGMR, 1983a, 1983b, 1991), which may be the cause for the later development of the Cenozoic Yushu-Nangqian thrust wedge (Fig. 3A).[1]

We observe no direct depositional contact between the Carboniferous and Triassic strata in the study area. Whether a major unconformity exists between the two units omitting the whole Permian unit is not clear. Because Permian strata lie unconformably over a Carboniferous sequence ~130 km west of Nangqian in the Zhaduo area (Qinghai BGMR, 1991), we assume that the Permian strata lie beneath the Nangqian out-of-sequence fault zone (Fig. 3A). The Cenozoic strata unconformably overlie Carboniferous-Triassic strata and may be in conformable contact with underlying Upper Cretaceous strata (Qinghai BGMR, 1983a, 1983b, 1991). They were deposited in four distinctive Paleocene-Eocene basins (i.e., Shanglaxiu, Xialaxiu, Niuguoda, and Nangqian)

[1]Figures 2 and 3 are on a separate sheet accompanying this issue.

(Fig. 2) during Paleogene contraction (Horton et al., 2002).

Structural Geology

Pre-Cenozoic versus Cenozoic Deformation

Pre-Cenozoic deformational history may be established by examining unconformable relationships between Cenozoic and pre-Cenozoic strata. The angular discordance between Cenozoic and underlying Paleozoic-Triassic strata is most prominent in the northernmost end of the mapped area against the Ganzi-Yushu fault, where lower Tertiary strata and underlying Triassic beds have opposite dip directions (Fig. 2). The discordance is also displayed along the northern edge of the Shanglaxiu basin, where pre-Cenozoic strata dip 10°–40° more steeply than the overlying Cenozoic strata. Despite the difference in dip angles, the two sequences generally share similar strikes (Fig. 2). The discordance between Cenozoic strata and underlying Triassic beds in the Xialaxiu basin is less obvious—dips of the two sequences above and below the unconformity are quite similar (Fig. 2). Variable discordant relationships between Jurassic and Cenozoic strata and between Carboniferous and Cenozoic strata are also observed along the southern margin of the Nangqian basin.

We found no clear evidence for the existence of major pre-Cenozoic faults across the region. The only possible candidate for pre-Cenozoic faults is the Jiangda thrust exposed ~15 km west of Nangqian (Fig. 2). The fault juxtaposes an older Carboniferous unit over a younger Carboniferous unit and itself is overlain by the uppermost part of the Paleocene-Eocene Nangqian basin strata (Fig. 2), suggesting motion between the Carboniferous and Eocene. However, even for this fault the evidence for major motion in the Paleocene is strong, as indicated by the distribution of proximal-facies sedimentation and a growth-strata relationship with folds against the fault (Horton et al., 2002). Because of the lack of evidence for major pre-Cenozoic faults in the region, we assume that the Cenozoic strata were unconformably deposited on top of broadly folded Carboniferous-Triassic strata (Fig. 3A). The pre-Cenozoic deformation along the northern margin of the Qiangtang terrane may have been related to Late Triassic closure of the Songpan-Ganzi remnant ocean (Yin and Nie, 1993, 1993; Nie et al., 1994; Şengör and Natal'in, 1996; Zhou and Graham, 1996), because the Cenozoic and Jurassic-Cretaceous strata are generally conformable in the area. In any case, pre-Cenozoic folding appears to have accommodated rather minor NE-SW shortening, perhaps no more than 2–3 km along the Yushu-Nangqian traverse, based on restoration of broad pre-Cenozoic folds.

Shanglaxiu Thrust System

The Shanglaxiu thrust system consists of (1) the southwest-dipping Shanglaxiu fault, (2) a 5–8-km-wide zone of folds in the Shanglaxiu basin in the footwall of the Shanglaxiu fault, and (3) several low-angle north-and-south–dipping thrusts located between the Shanglaxiu basin to the south and the Ganzi-Yushu fault to the north (Figs. 2, 3A, 4, 5A, and 5B). The trace of the Shanglaxiu fault is overlain by Lower Eocene strata, which are themselves deformed by northwest-trending folds coaxial with earlier folds in the hanging wall and footwall of the thrust (Figs. 2 and 4).

The Shanglaxiu fault dips 20°–30° to the south and juxtaposes a Triassic carbonate sequence (T_3jz^2) over Paleocene–Lower Eocene strata (E_S^1). Due to the reconnaissance nature of our mapping, we did not examine the kinematics of the Shanglaxiu fault zone in detail. Nevertheless, we interpret the fault to be a major northeast-directed thrust based on: (1) the consistent older-over-younger relationship (Fig. 4), (2) a parallel relationship between the fault and northeast-verging and locally overturned folds exposed immediately above and below the fault (Fig. 4), (3) its low-angle geometry, and (4) locally preserved growth-strata relationship between the Shanglaxiu fault and its footwall folds (Horton et al., 2002).

North- and south-dipping thrusts north of the Shanglaxiu thrust juxtapose the lowest Triassic units (T_3jz^1 sandstone and T_3jz^2 carbonate) over equivalent or younger Triassic strata. They also thrust Triassic strata over the distal facies of the Paleogene Shanglaxiu basin (Figs. 2 and 3A). Fault striation on one thrust trends southwest (fault 18 in Figs. 2 and 6).

In map view the Shanglaxiu thrust makes an abrupt change in strike of ~70° from a northwest trend to nearly north-south direction (Figs. 2 and 4). Correspondingly, the footwall folds make a similar turn in the trend of fold axes. This map pattern may result from oroclinal bending under distributed right-slip shear across a broad (>10-km-wide) northwest-trending deformation zone. The inferred oroclinal bending may explain the peculiar observation that fault striations along the north-striking segment of the Shanglaxiu fault trend westward (Fig. 4) (see fault 11 in Figs. 2 and 6).

The Triassic strata in the Shanglaxiu hanging wall are folded, with a wavelength of 1–1.5 km and amplitude of several hundred meters (Figs. 2 and 4). The northeast-verging folds close to the Shanglaxiu thrust are locally overturned and accommodated ~50% of shortening strain. These folds are probably Cenozoic in age because they are parallel to footwall Cenozoic folds and have vergence consistent with northeastward thrusting.

Shanglaxiu Back Thrust

The Shanglaxiu back thrust places older Triassic units (T_3jz^1, T_3jz^2) over younger Triassic units (T_3jz^3, T_3jz^4) (Figs. 3 and 4), with a maximum stratigraphic separation of ~4 km. This fault dips at an angle <35° to the northeast and is locally overlain by Lower Eocene volcanic flows dated as 51–49 Ma (Roger et al., 2000; this study, see following) (Fig. 2). The volcanics overlie the Shanglaxiu back thrust and are deformed by northwest-trending folds.

Fault striations on the main fault surface (fault 15 in Fig. 6) and asymmetric folds in the fault zone indicate SW-directed motion. The back thrust is parallel to a zone of tight folds in Triassic strata in both the hanging wall and footwall. In the footwall, these folds are locally overlain by gently folded Tertiary strata, which are in turn cut by a southwest-dipping fault preserving subhorizontal striations (fault 10 in Fig. 6).

Xialaxiu Thrust

The Xialaxiu fault is folded and roots to the south. It juxtaposes Triassic strata (T_3jz^1, T_3jz^2) over Paleogene deposits of the Xialaxiu basin (E_X) and Triassic unit T_3jz^2 (Fig. 2). We have no constraints on the thrust transport direction, but based on its similar strike to the Shanglaxiu thrust, an older-over-younger relationship, parallelism between the fault and footwall folds, and the low-angle geometry, we suggest that this is also a northeast-directed thrust. In cross-sectional view, we interpret the fault to be a hanging-wall flat following the base of T_3jz^1 sandstone (Fig. 3A). In map view, the fault cuts upsection in hanging-wall strata laterally to the southeast.

The hanging wall and footwall of the Xialaxiu thrust are folded together (Fig. 2), which may be attributed to motion on a minor northeast-directed thrust (Figs. 2 and 3A). Minor, northeast-directed thrusts are present a few kilometers north of the northern margin of the Xialaxiu basin, ~4 km south of the Shanglaxiu back thrust (Fig. 2).

Niuguoda Thrust

The northeast-dipping Niuguoda fault juxtaposes a Triassic unit (T_3jz^2) over Paleogene deposits of the Niuguoda basin (E_{NU}) and Triassic unit T_3jz^3 (Figs. 2 and 3A). Similar to the thrusts described above, this fault is also folded producing an irregular map pattern. At one location, the fault exhibits north-trending

Geologic Map of the Yushu-Nangqian Region East-central Tibet

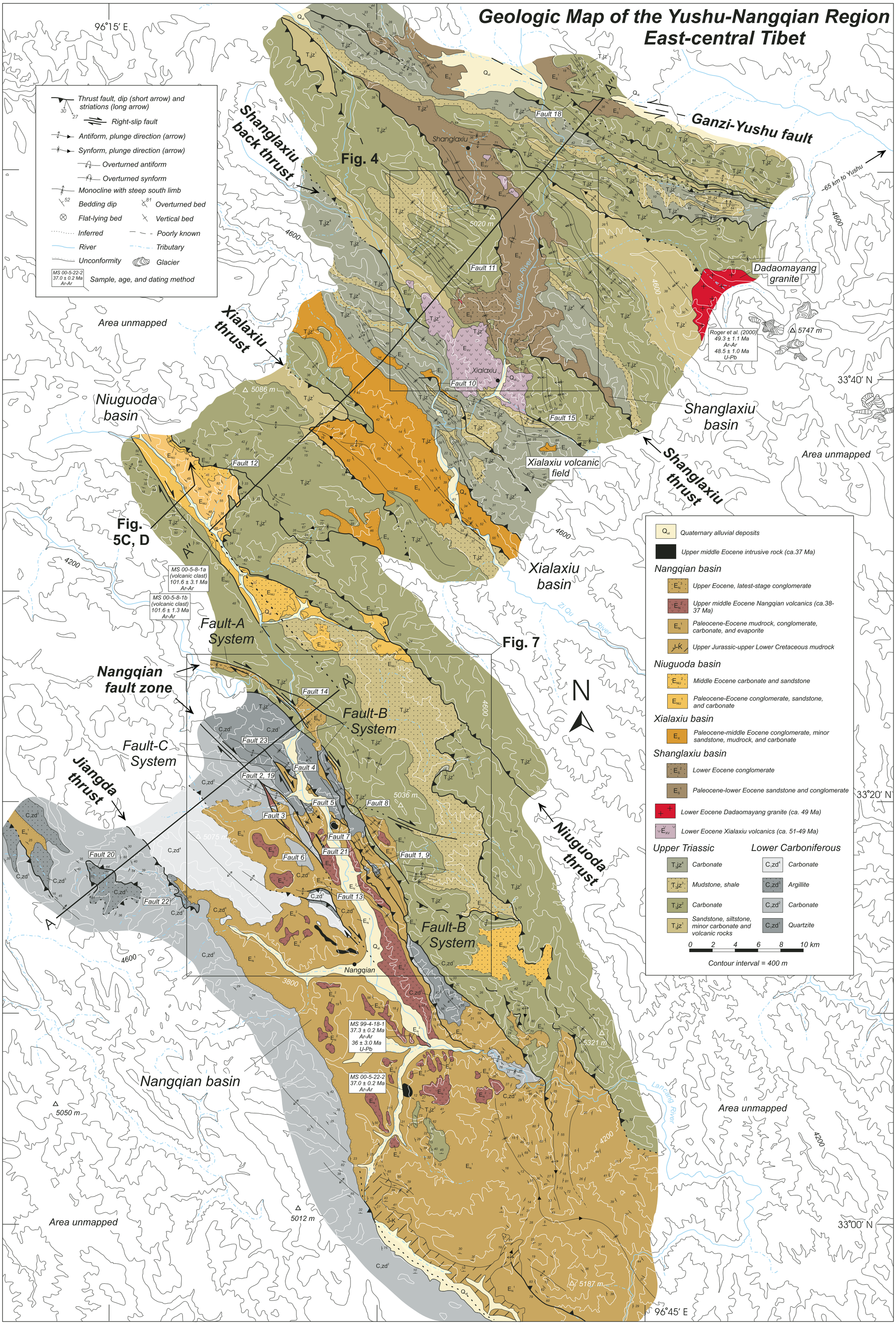

Figure 2.

Figure 2. Geologic map of the Yushu-Nangqian area depicting structures and rock types of Carboniferous-Triassic rocks and four outcrop belts of overlying Cretaceous-Paleogene syncontractional deposits, after Qinghai BGMR (1983a, 1983b) and our own observations. Location of photos (Fig. 5C–D) also shown.

Structural evolution of the Yushu-Nangqian region and its relationship to syncollisional igneous activity, east-central Tibet
Matthew S. Spurlin, An Yin, Brian K. Horton, Jiangyu Zhou, and Jianghai Wang
Figures 2 and 3
Supplement to: *Geological Society of America Bulletin*, v. 117, no. 9/10

1. 15° southwest dip of frontal ramp is constrained by tilted Paleogene bedding in the overlying Shanglaxiu basin.
2. Inferred basal décollement within T_3jz^1 sandstone in the northern portion of the study area is based on the recurrence of this unit as the oldest unit repeatedly exposed in thrust hanging walls (Figure 2) and from observed hanging-wall flat geometries (see points 4 and 5).
3. Isoclinally folded hanging-wall strata between the Shanglaxiu thrust and Shanglaxiu back thrust suggest as much as 50% internal strain within the thrust sheet, independent of the translation.
4 and 5. The observed hanging-wall flat within T_3jz^1 sandstone suggests a minimum of 18 km of reverse slip along the Xialaxiu thrust and footwall imbricate thrust. Its associated footwall-flat lies structurally and stratigraphically above Carboniferous strata exposed at the surface along A-A'. We therefore infer that the root of the Niuguoda and Xialaxiu thrusts, which must project above the surface (point 5), is the Jiangda thrust.
6. Thrust fault projected onto line of section from southeastern part of the Xialaxiu basin. Minor slip on this structure is responsible for folding of both the hanging-wall and the footwall of the Xialaxiu thrust.
7. T_3jz^3 thickens stratigraphically from 450 m in the north (near Shanglaxiu) to 1300 m in the south beneath the unconformably overlying Tertiary strata of the Niuguoda basin (see Figure 2).
8. 45° northeast dip of the lowest part of the Nangqian thrust ramp is constrained by tilted Paleogene bedding in the overlying Niuguoda basin.
9. Out-of-sequence slip on the south-vergent Nangqian thrust along the frontal limb of an inferred, north-vergent fault propogation fold explains the apparent younger-over-older thrust relationship observed on the eastern margin of the Nangqian basin (see Figures 2 and 6). The timing of out-of-sequence slip is constrained by ca. 37 Ma Ar-Ar ages of volcanic rocks that are interbedded with syncontractional strata of the Nangqian basin and cut by the Nangqian thrust.
10. Permian strata unconformably overlie C_1zd^1 and C_1zd^2 locally (Qinghai BGMR, 1983a).
11. Top of footwall ramp constrained by inferred Permian hanging wall-cutoff shown in A-A' and our minimum estimate of ~46 km of cumulative slip on the basal décollement northeast of this point.

[Note: Thicknesses of Carboniferous-Permian units are poorly constrained and are based partially on dip data from our geological mapping and from previous work (Qinghai BGMR, 1983a, 1983b).]

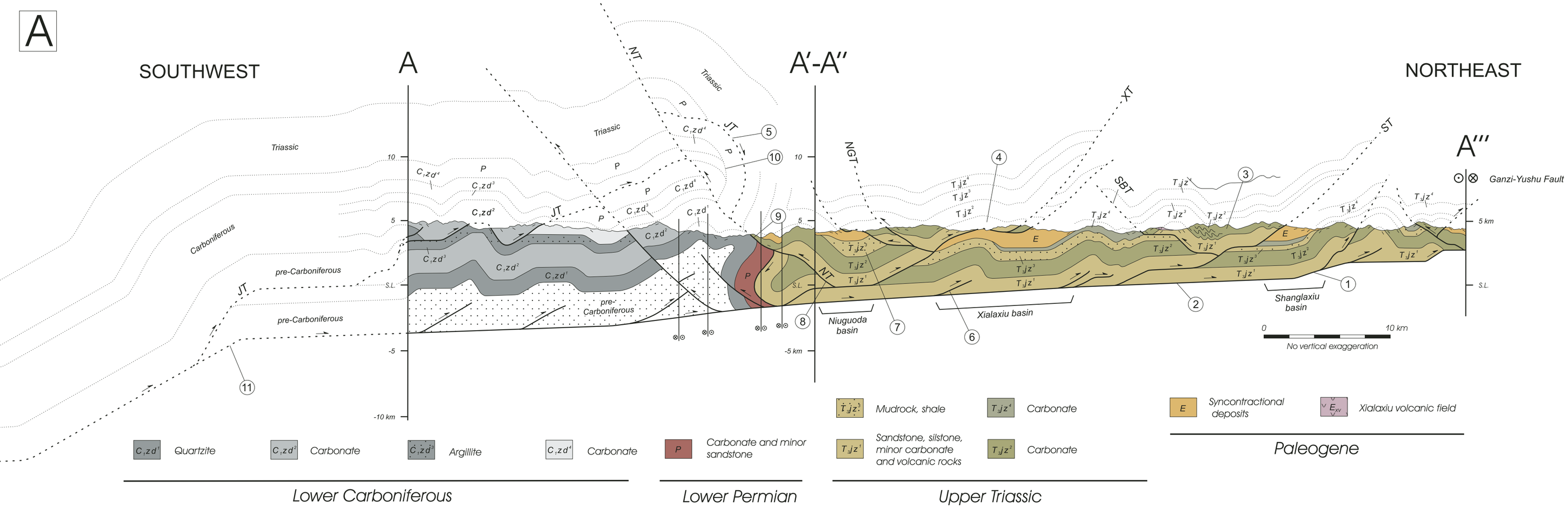

FAULT ABBREVIATIONS:
ST = Shanglaxiu thrust
SBT = Shanglaxiu back thrust
XT = Xialaxiu thrust
NGT = Niuguoda thrust
NT = Nangqian thrust
JT = Jiangda thrust

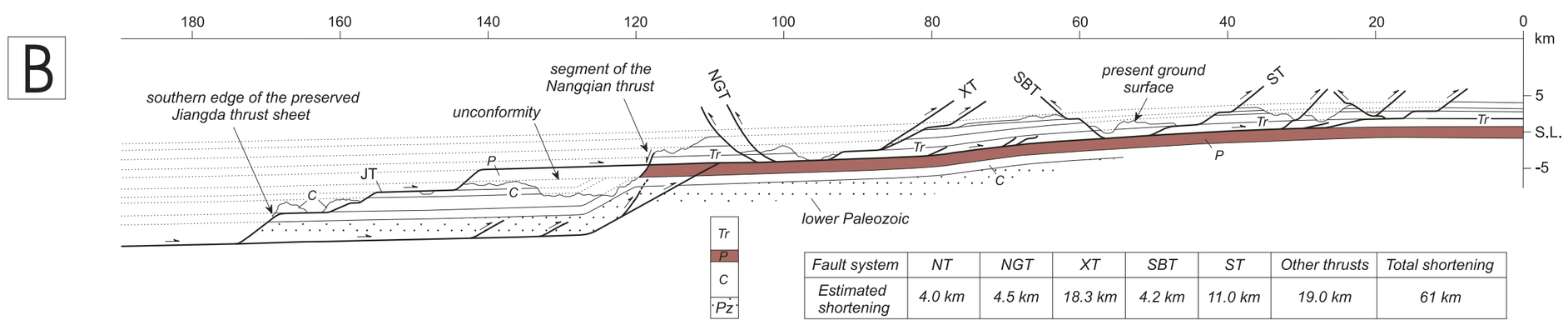

Fault system	NT	NGT	XT	SBT	ST	Other thrusts	Total shortening
Estimated shortening	4.0 km	4.5 km	18.3 km	4.2 km	11.0 km	19.0 km	61 km

Figure 3. (A) Balanced cross section of thin-skinned deformation and syncontractional basin development associated with Paleocene-Eocene shortening in the Yushu-Nangqian region. Numbers refer to annotations listed at the top of the figure. (B) Restored cross-section A–A″. The tabulation at lower right provides shortening estimates for individual faults and fault systems. Abbreviations are as follows: ST—Shanglaxiu thrust; SBT—Shanglaxiu back thrust; XT—Xialaxiu thrust; NGT—Niuguoda thrust; NT—Nangqian thrust; JT—Jiangda thrust. See text for details. S.L.—sea level.

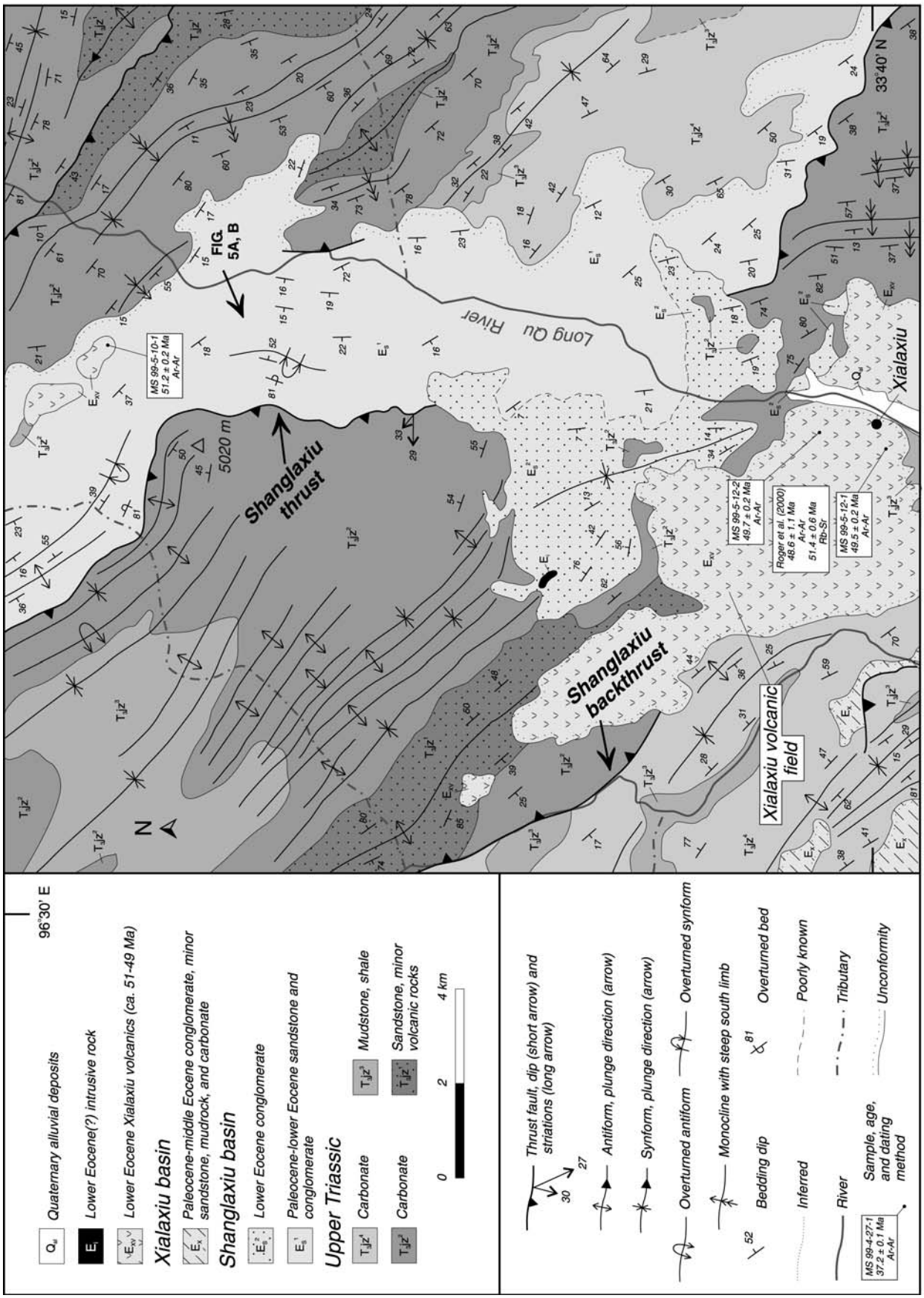

Figure 4. Geologic map of the Shanglaxiu area (see Fig. 2 for regional location). Location of photos (Fig. 5A–B) also shown.

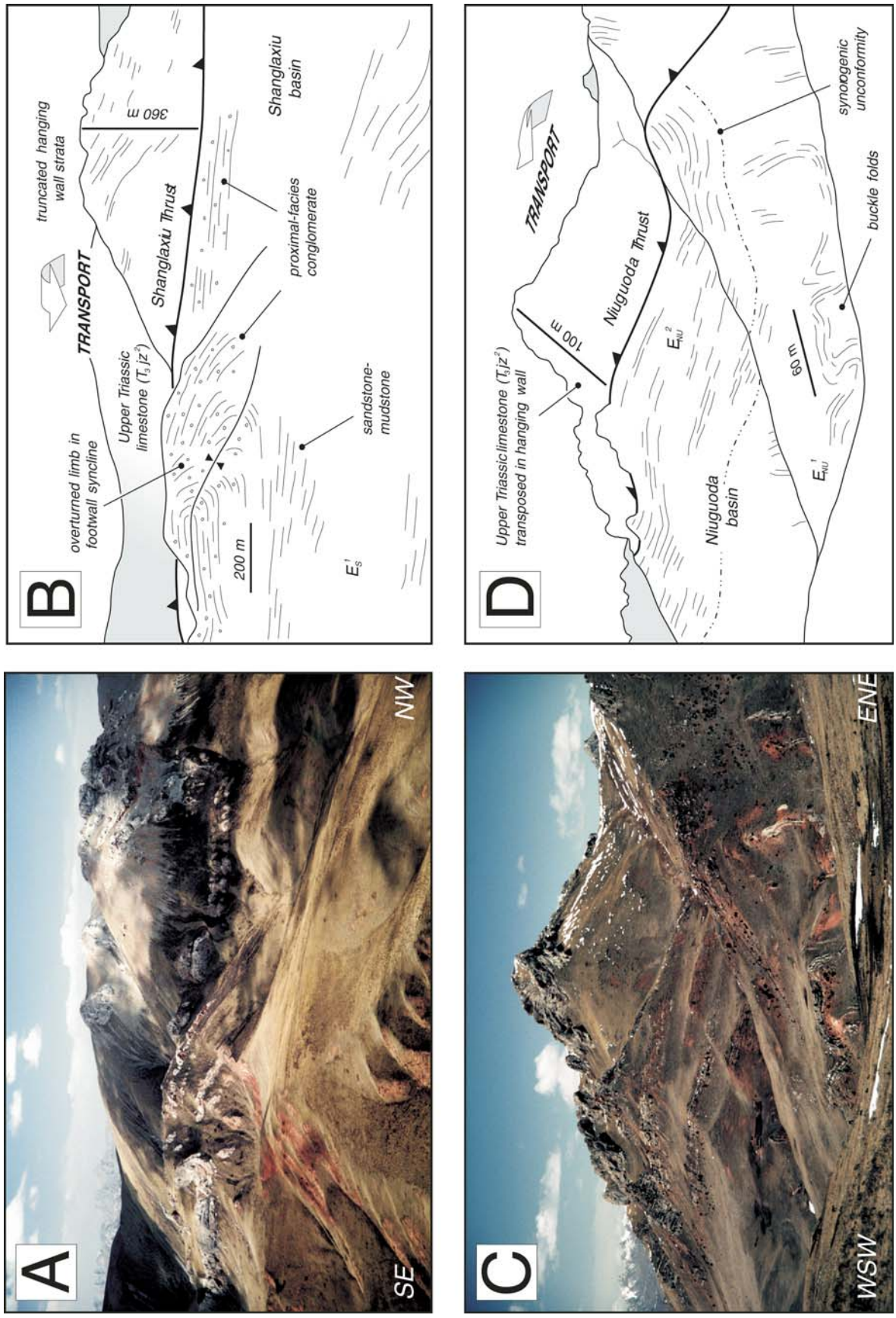

Figure 5. Paleocene-Eocene thrust structures within the northern and central portions of the Yushu-Nangqian traverse. (A) Photograph and (B) line drawing of the northeast-directed Shanglaxiu thrust and associated syncontractional deposits of the Shanglaxiu basin. Note the truncation of Triassic carbonate (T_3jz^2) in the hanging wall of the Shanglaxiu thrust and a well-developed footwall syncline (with partially overturned strata) associated with thrust motion to the east-northeast. See Figure 4 for photo location. (C) Photograph and (D) line drawing of the southwest-directed Niuguoda thrust. Footwall rocks consist of intercalated mudrock and lacustrine limestone of the Niuguoda basin. A local synorogenic unconformity attests to the syncontractional nature of the underlying footwall rocks, which are highly folded as a result of slip on the Niuguoda thrust. See Figure 2 for photo location.

striations along its north-striking segment (fault 12 in Fig. 6). This observation together with the older-over-younger relationship indicates that the fault transport direction was southwestward in present coordinates.

Nangqian Fault Zone

The northwest-trending Nangqian fault zone is a composite structural assemblage formed during several phases of deformation. For the convenience of description, we break the fault zone into three small fault systems (Figs. 2 and 7), each of which in turn consists of small splays and complex arrays that may have different kinematics and may have been formed at different times. Proposed ages of fault activity are based on assigned stratigraphic ages (Qinghai BGMR, 1983a). Where possible, we utilize our new age determinations on igneous rocks. However, timing along the Fault-A and Fault-B systems is based on age assignment of Upper Eocene unit E_N^3 by Qinghai BGMR (1983a), for which we do not have independent verification.

Fault-A System. Fault-A in the northwestern end of the fault zone strikes east and dips 40°S. Fault striations plunge gently (17°) to the west, indicating dominant strike-slip motion and a minor normal-slip component (Fig. 7). The fault places younger Upper Eocene strata (E_N^3) over older Triassic units (Fig. 7). Although the Fault-A system cuts E_N^3, the Eocene unit directly against the fault exhibits growth-strata relationship, suggesting that motion along the fault and deposition of the unit were related. To the southeast, this fault splits into two strands. The northern strand cuts unit E_N^3, whereas the southern strand dies out into a fold in unit E_N^3. The southern strand is high-angle and preserves mostly subhorizontal striations (fault 14 in Fig. 6). The offset pattern of unit E_N^3 (Fig. 7) indicates the Fault-A system to be right-slip with total slip <2 km.

Fault-B System. The northwestern end of the Fault-B system immediately south of the Fault-A system consists of a single strand striking east. The fault dips north and places a younger Triassic unit (T_3jz^2) over older Carboniferous strata, omitting several younger Carboniferous units and the basal Triassic unit T_3jz^1 (Fig. 2). To the southeast the fault changes strike to the northwest and is overlain by a folded Upper Eocene unit E_N^3 (Fig. 7), suggesting that it had ceased motion by late Eocene time. The Fault-B system is older than the Fault-A system, because the latter cuts E_N^3.

To the southeast Fault-B splits into two splays. The northern branch is nearly vertical and exhibits a sharp contact between Tertiary red beds to the northeast and Triassic carbonate in the south. The fault dies out into the Triassic strata. The

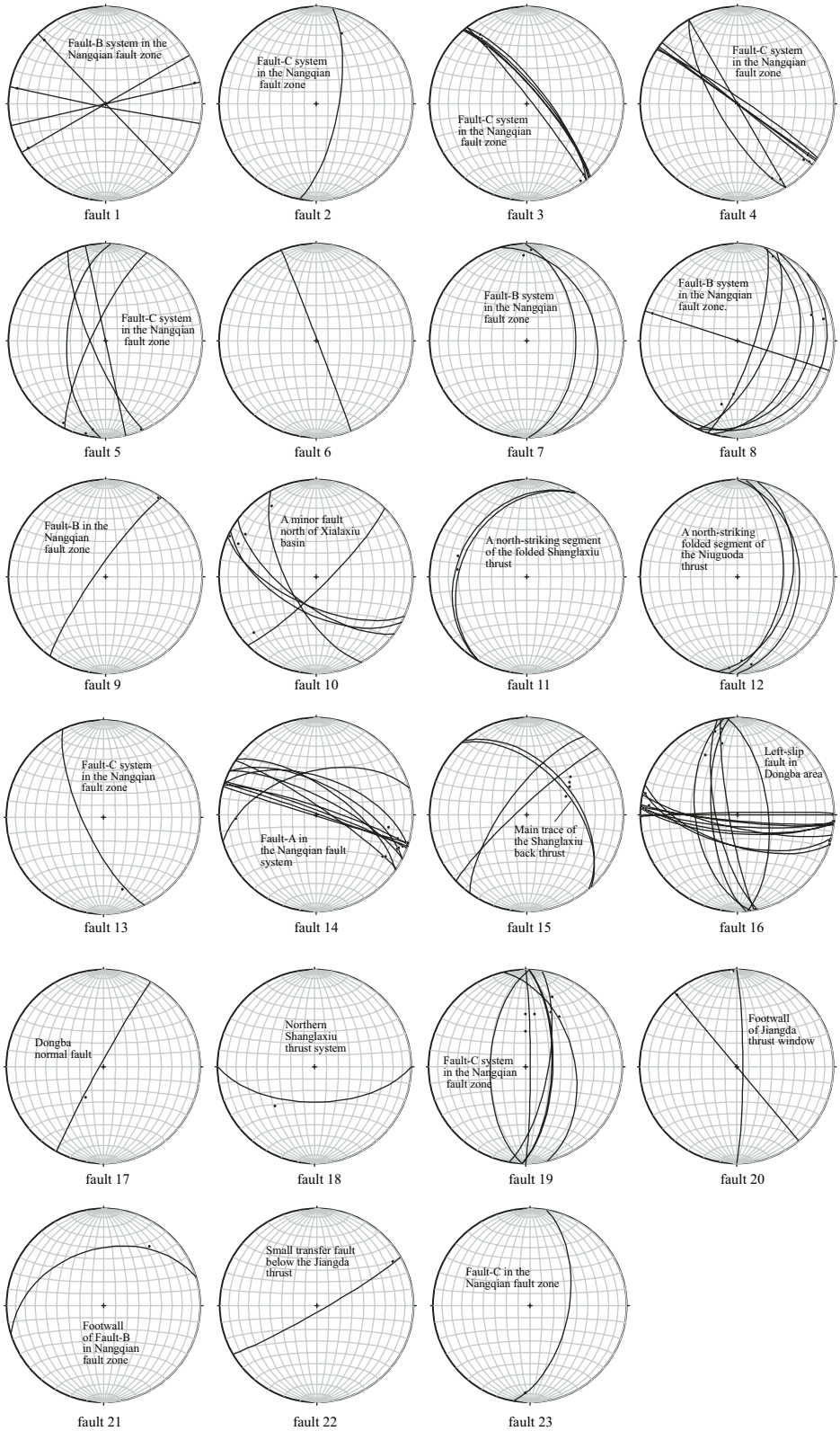

Figure 6. Fault kinematic data. See Figure 2 for location and text for details. Note that some striations are not exactly on the corresponding fault surfaces. This is due to the fact that fault surfaces are highly irregular in places and only average measurements are used to represent fault attitudes.

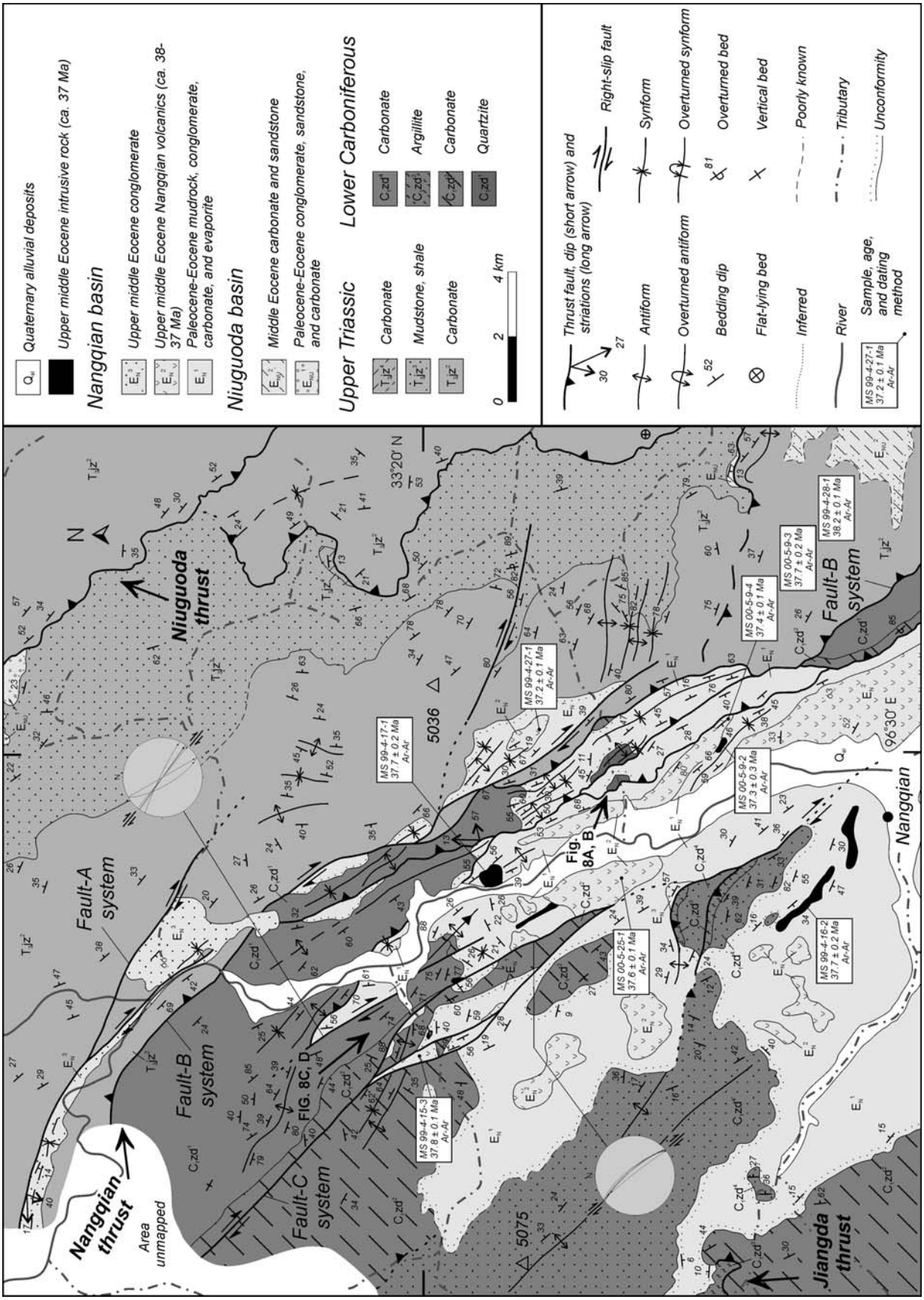

Figure 7. Geologic map of the Nangqian area (inset from Fig. 2). Location of photos (Fig. 8) also shown.

fault zone is observed at locations of fault 1 and fault 8 (Figs. 2 and 6). Fault 8 is east-dipping and preserves both nearly down-dip east-trending lineation and subhorizontal north-trending lineation. Fault 1 exhibits subhorizontal striation, and Tertiary beds within 1–3 m from the fault contact are consistently offset left laterally for ~20–50 cm, suggesting left-slip motion on fault 1. Our local observation of fault kinematics appears to be incompatible with the regional map pattern for the northern fault strand, which seems to indicate right-lateral motion for the fault. First, Tertiary unit E_N^1 is offset for ~1.5 km right laterally. Second, an en echelon fold pattern in E_N^1 directly against the fault is consistent with right-slip shear. Third, the fault terminates into a series of east-trending folds at its southeastern end, a relationship requiring the fault to be right-slip. The contradictory observations may be explained by the fault zone experiencing both left-slip and right-slip motion. Perhaps the right-slip motion is more dominant, producing the map-scale structures and followed by minor and local left-slip reactivation. Alternatively, folds adjacent to and at the termination of the fault could be unrelated to faulting. In this case, Tertiary unit E_N^1 was deposited during left-slip faulting and the apparent right-lateral offset pattern of E_N^1 is due to a complex original distribution of individual localized basins. This latter hypothesis can be tested by further detailed sedimentological studies.

The southern branch of the Fault-B system dips moderately to steeply (50°–70°) northeastward and juxtaposes Carboniferous units over Paleogene strata (E_N^1 in Fig. 2). Imbricate faults in its footwall cut 37 Ma Eocene volcanic flows (E_N^2) (Fig. 2). Tight folds involving Tertiary strata are directly below the main trace of the southern branch of Fault-B and parallel to the fault (Fig. 7). Small thrusts are also preserved in the fold zone, such as fault 7 (Figs. 2 and 6); striations on these faults dominantly trend northeast, consistent with NE-SW contraction. In contrast, gentle (13°) to moderate (45°) north-plunging striations are observed on the main trace of the southern fault branch (Fig. 7), indicating the fault has a significant strike-slip component. Fault 9 (Figs. 2 and 6) in the main southern fault zone could be a minor conjugate fault. The sense of slip on the southern fault strand is unclear. However, based on the regional map pattern, we suggest that it is left-slip. This is because the fault terminates in the southeast into a series of north-trending folds in the Paleogene Nangqian basin. The north-trending folds caused northward concave bending of a prominent NW-trending anticline, suggesting that left-slip motion along the southern fault branch postdates the NE-SW contraction.

Fault-C System. The northwest-striking Fault-C system in the southwestern part of the Nangqian fault zone consists of several nearly vertical fault branches striking northwest (Fig. 8). They mainly follow the course of the Lacang River. For this reason we also refer to this fault system as the Lacang fault system. The main fault strand juxtaposes Paleogene red beds to the northeast and highly folded Triassic strata to the southwest. Its strike changes southeastward from northwest to north. In contrast to the parallel fault-fold relationship along the Fault-B system, the Fault-C system cuts and offsets several northwest-trending folds, which may have formed during the development of the Fault-B system. The Fault-C system also cuts the 37 Ma Nangqian igneous complex (Fig. 8). Striations measured in the Fault-C system (faults 2, 3, 4, 5, 6, 13, 19, and 23 in Fig. 6) are all subhorizontal, indicating dominant strike-slip motion. One fault branch in the Fault-C system offsets the unconformity between Carboniferous and Paleogene strata right laterally for 120–130 m (Fig. 8C and 8D). Several vertical northwest-striking faults directly north of Nangqian can be traced into east-striking low-angle thrusts, indicating right-slip motion on the vertical faults (Fig. 7). However, left-slip fault motion has also been observed. For example, fault 19 and fault 5 are parts of a major vertical fault striking northwest. They juxtapose Tertiary strata against Carboniferous strata. Near the fault 19 location, minor faults in the fault zone are north-striking and preserve subhorizontal striations. Drag folds and offset of beds by small faults next to the main fault zone all indicate left-slip kinematics. The preceding observations suggest that the Fault-C system may have also experienced two phases of strike-slip faulting. However, it is not clear if the left-slip faulting is older or younger than right-slip faulting in the fault system.

Summary. The preceding observations suggest a complex deformation history. In particular, the Fault-B system may have been reactivated several times in the past. The close association between the southern fault strand in the Fault-B system with parallel folds and its consistent north dip suggest that it may have originated as a thrust. Contradictory kinematics suggest that this fault zone has experienced both right-slip and left-slip faulting, with the former occurring first, possibly coeval with NE-SW contraction. The crosscutting relationship with respect to unit E_N^3 also helps bracket deformational events. Based on the field observations and preceding discussion, a possible sequence of deformation in the Nangqian fault zone is proposed: (1) NE-SW contraction that produced northwest-trending folds in the Nangqian basin, (2) coeval or slightly younger right-slip faulting along the northern fault branch of the Fault-B system that produced en echelon folds and east-trending folds at the southwest fault termination, (3) left-slip faulting along the southern fault branch of the Fault-B system that locally reactivated the northern fault branch of the Fault-B system, produced north-trending folds at its southwestern termination and deformed the older northwest-trending folds, (4) deposition of Upper Eocene unit E_N^3, which was subsequently folded due to NE-SW contraction, and (5) development of the Fault-A system that cuts E_N^3. The proposed sequence of deformation implies two distinctive phases of right-slip faulting and two phases of NE-SW contraction.

Jiangda Thrust

The Jiangda thrust juxtaposes an older Carboniferous unit (C_1zd^2) over a younger Carboniferous unit (C_1zd^3) (Figs. 2 and 8). A folded thrust window juxtaposing the same units is exposed ~3 km southwest of the frontal trace of the Jiangda thrust, where the fault zone consists of a 40-m-thick cataclastic zone. The frontal trace of the thrust is overlain to the south by Nangqian basin strata (E_N^1) (Fig. 7), which constrains the thrust to predate the late Eocene. Sedimentologic investigations along the southern margin of the Nangqian basin suggest that the Jiangda thrust was active during the early stage of basin development in the Paleocene (Horton et al., 2002). The Jiangda thrust may reappear again ~15 km due south of Nangqian, where a southwest-dipping thrust juxtaposes Carboniferous unit C_1zd^2 over Jurassic and Cretaceous strata (Fig. 2).

Folds and thrusts involving Carboniferous strata are also present between the Jiangda thrust in the south and the Nangqian fault zone in the north (Fig. 2). A broad northwest-trending antiform defined by unit C_1zd^4 is located 7 km northwest of Nangqian (Fig. 2). This fold may be associated with blind thrusting at depth (Fig. 3A). Directly north of Nangqian, Carboniferous units (C_1zd^4, C_1zd^3) are thrust along two south-dipping imbricate thrusts over lacustrine deposits of the Nangqian basin (E_N^1) and a local apron of Paleogene conglomerate related to thrusting (E_N^3).

Kinematic data on the Jiangda faults are sparse. One small left-slip high-angle fault is observed directly below the Jiangda thrust (fault 22 in Fig. 6). If this fault is a transfer structure in a contractional system, it implies that the Jiangda thrust is a northeast-directed structure. In the Jiangda thrust window to the southwest, two mesoscopic high-angle faults lie below the low-angle Jiangda thrust. They preserve subhorizontal striations and right-slip-sense kinematic indicators. It is not clear how these high-angle

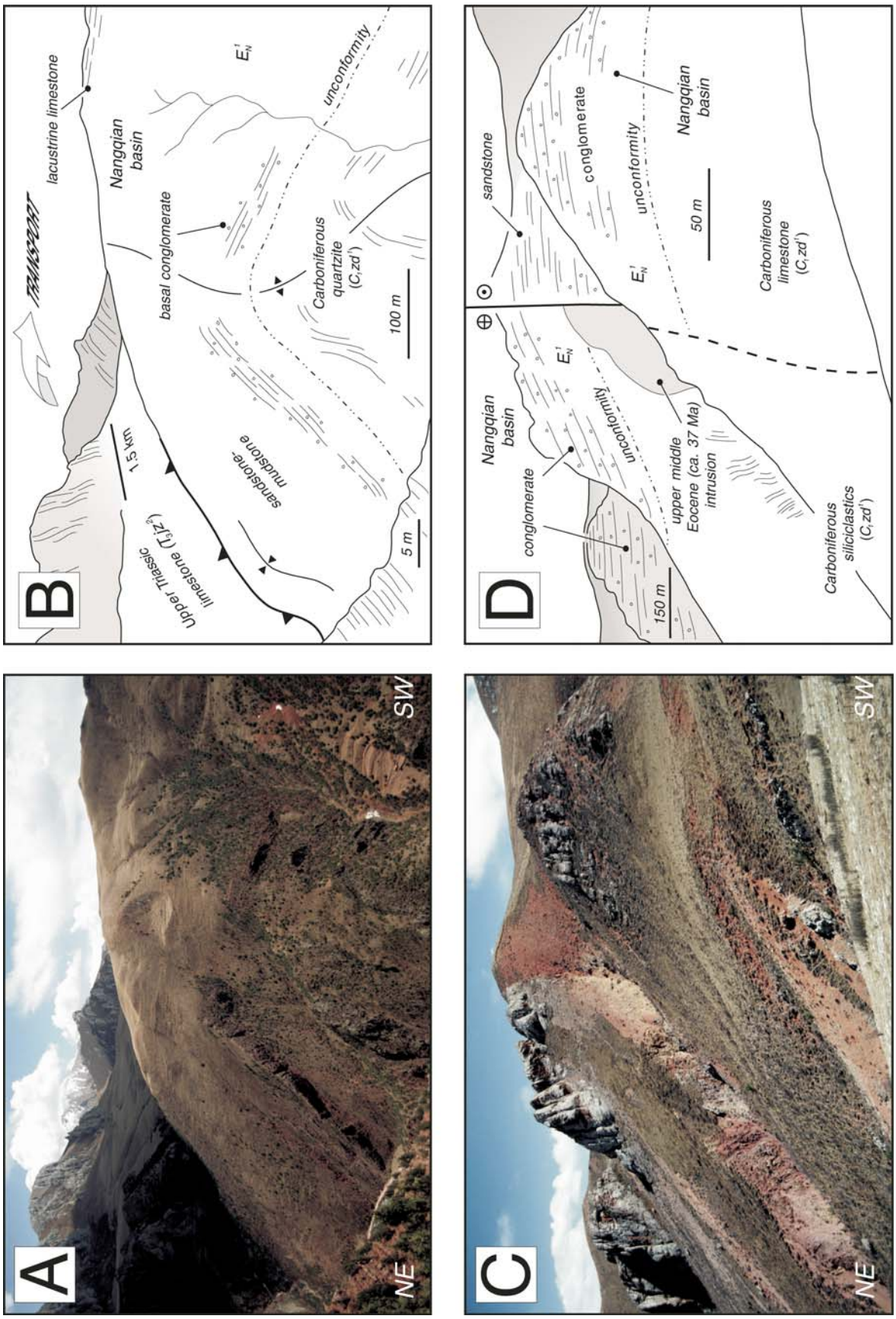

Figure 8. Paleocene-Eocene fault structures in the Nangqian area. See Figure 7 for photo locations. (A) Photograph and (B) line drawing of the southwest-directed Nangqian thrust, a major basin-bounding feature along the northeastern margin of the Nangqian area. Folding of the Carboniferous-Paleogene rocks in the footwall of the Nangqian thrust resulted from footwall imbrication and surface-rupture of an additional thrust located ~1 km to west (to the right) of this photo during a younger episode of southwest-directed thrusting. (C) Photograph and (D) line drawing of right-lateral offset of an upper middle Eocene intrusion and south-dipping Tertiary unconformity between underlying Carboniferous strata and overlying Paleogene red clastic strata of the lower Nangqian basin.

faults below were related to motion on the low-angle Jiangda thrust. If the high-angle faults are small transfer structures, the thrust transport direction for the south-dipping Jiangda fault is to the south.

GEOLOGY OF THE DONGBA AREA

We conducted reconnaissance mapping in the Dongba area to examine the lateral continuity of the Yushu-Nangqian thrust belt (Figs. 1 and 9). The area exposes the north-dipping Cenozoic Dongba thrust that puts Carboniferous units over strata that are mapped as Neogene in age (Qinghai BGMR, 1988). Neogene strata in the Dongba basin generally dip homoclinally to the north. However, as they approach the Dongba thrust, the strata become folded and form a series of short-wavelength (<1 km) synclines and anticlines parallel to the thrust. In the northern Dongba area, Neogene strata rest directly on top of Carboniferous strata, missing Permian and Triassic rocks. Because the age of this unconformity is unknown, it is not clear whether the Permian and Triassic strata were eroded away in the Mesozoic or during Cenozoic thrusting. The maximum total stratigraphic throw across the Dongba thrust is ~4–5 km, assuming a continuous Carboniferous to Triassic section directly above the thrust. If we further assume that the Dongba thrust dips ~30°, its maximum slip is at least 8–10 km. Taking the Neogene age assignment by Qinghai BGM (1988) at face value, the field relationships imply significant contractional deformation in the Yushu-Nangqian thrust belt that occurred either episodically or continuously from the Paleogene to Neogene over a time span of perhaps more than 30 m.y.

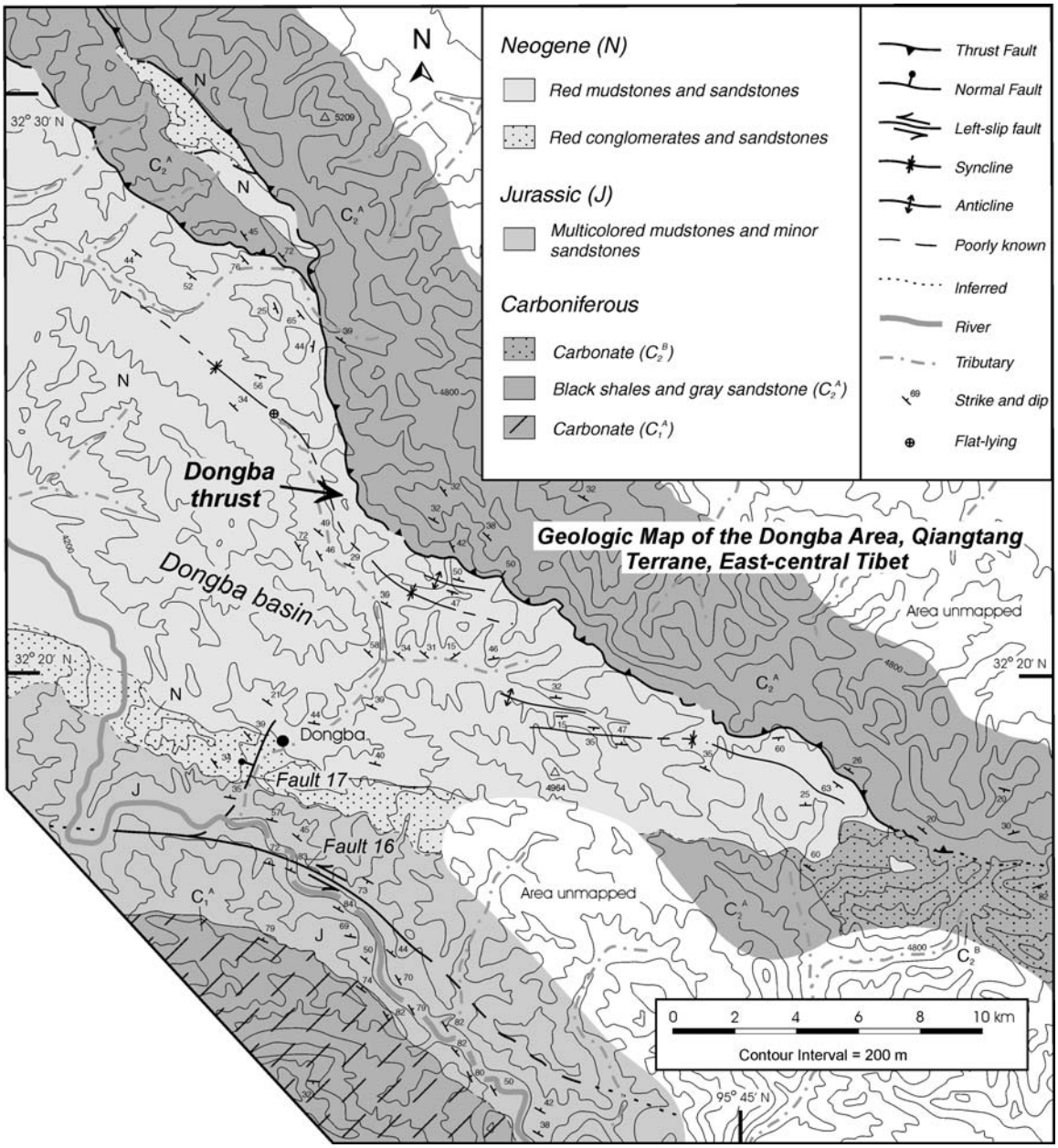

Figure 9. Geologic map of the Dongba area.

A prominent left-slip fault occurs along the southern margin of the Dongba basin (Fig. 9). Striations on minor faults parallel to the main fault surface are subhorizontal and left-slip (fault 16 in Fig. 6). Because it lies entirely in the Jurassic strata, we are uncertain whether this fault is a Cenozoic or Mesozoic structure. Immediately west of the town of Dongba, we observe a west-dipping high-angle normal fault that cuts the Dongba Neogene strata (Fig. 9; fault 17 in Fig. 6). This fault appears to merge with the left-slip fault to the south. However, we are uncertain whether the two faults join each other or crosscut one another.

GEOLOGY OF ZHADOU AREA

The Zhaduo area ~130 km west of Nangqian (Figs. 1 and 10) consists of a series of northwest-striking thrusts that dip both to the northeast and southwest. Tertiary strata rest unconformably on top of Cretaceous and Permian strata. Tight folds are present in the Carboniferous units above or below the major thrusts. It is not clear whether these folds formed during the Cenozoic or Mesozoic. The style of deformation in the Zhaduo area generally mimics that along the Yushu-Nangqian traverse, indicating that the observed thrust belt is laterally continuous for at least 130 km west of the Yushu-Nangqian region.

The Zhaduo area preserves the best evidence for Cenozoic out-of-sequence thrusting. In the northeastern corner of the mapped area, a north-dipping thrust places a younger Triassic unit (T_3jz^2) over a Permian unit (P_1z^2). The same fault also thrusts Triassic strata over a Paleocene unit (E_d), clearly indicating Cenozoic thrusting on the fault. This younger-over-older relationship is similar to what we observed along the Nangqian fault zone (i.e., the southern branch of the Fault-B system) and lends support to our speculation that the Permian unit is continuous along the Yushu-Nangqian traverse, but is buried by an out-of-sequence thrust near Nangqian (Fig. 3A).

CENOZOIC IGNEOUS ACTIVITIES

Cenozoic igneous rocks are widely distributed in central and eastern Tibet (e.g., Liu, 1988; Deng, 1989, 1998; Pan et al., 1990; Turner et al., 1993; Roger et al., 2000; Wang et al., 2001). In the Yushu-Nangqian region, Paleogene igneous rocks were known at least two decades ago (Qinghai BGMR, 1983a, 1983b, 1991). In the Xialaxiu area, Roger et al. (2000) dated Xialaxiu volcanic flows using the Rb-Sr method. Their isochron defined by whole rock, K-feldspar, and four biotite fractions yields an age of 51.4 ± 0.6 Ma. The $^{40}Ar/^{39}Ar$ dating of the volcanic flow by the same authors yields a 48.6 ± 1.1 Ma total fusion age. A block of glacial float presumably derived from the Dadaomayang granite ~15 km east of the Xialaxiu volcanic field was also dated by Roger et al. (2000), which yields a U-Pb age of 48.5 ± 1.0 Ma and an Ar/Ar biotite total fusion age of 48.6 ± 1.1 Ma. Our mapping shows that the Dadaomayang granite truncates a Tertiary thrust (Fig. 2). In the Nangqian area (Fig. 7), volcanic rocks unconformably overlie and are interbedded locally with the uppermost levels of the Nangqian basin strata (Horton et al., 2002). Intrusive rocks crosscut Cenozoic strata in the Nangqian basin zone (Fig. 7).

GEOCHRONOLOGY

$^{40}Ar/^{39}Ar$ Methods

Sixteen volcanic and plutonic samples were analyzed at the University of California–Los Angeles (UCLA) using $^{40}Ar/^{39}Ar$ thermochronology. Hand-selected biotite (~1–10 mg) and whole-rock aliquots (~18–23 mg) were wrapped in Cu foil and packed along with Al-wrapped Fish Canyon sanidine (FCT-1: 27.8 ± 0.3 Ma) flux monitors in 6 mm ID quartz tubes that were evacuated and sealed. Samples were irradiated at the University of Michigan's Ford reactor (L67 position). McDougall and Harrison (1999) provide more information regarding this facility and $^{40}Ar/^{39}Ar$ irradiation procedures. Correction factors for reactor-produced K- and Ca-derived argon were determined by measuring K_2SO_4 and CaF_2 salts included with each irradiation. The irradiation history, data of $^{40}Ar/^{39}Ar$ analysis, and all irradiation parameters (J, $^{40}Ar/^{39}Ar_K$, $^{38}Ar/^{39}Ar_K$, $^{36}Ar/^{37}Ar_{Ca,}$ and $^{39}Ar/^{37}Ar_{Ca}$) are available in the GSA Data Repository.[2]

Biotites and whole-rock aliquots were incrementally heated in a double-vacuum Ta furnace (see Lovera et al., 1997). Evolved gas was transferred by expansion and purified with an SAES ST-101 10 l/s getter pump. Gas delivery to the mass spectrometer was governed by splitting, using precalibrated procedures. Argon isotopic measurements were performed with an automated VG1200S quadrupole mass spectrometer. This instrument is equipped with a Baur-Signer source and an electron multiplier (see Quidelleur et al., 1997; Harrison et al., 2000).

Values of $^{40}Ar/^{39}Ar$, $^{38}Ar/^{39}Ar$, $^{37}Ar/^{39}Ar$, and $^{36}Ar/^{39}Ar$ ratios were corrected for total system backgrounds, mass discrimination (monitored by measurement of atmospheric Ar introduced by a pipette system), abundance sensitivity, and radioactive decay. Correction of $^{40}Ar/^{39}Ar$ ratios for nuclear interferences and atmospheric argon, and calculation of apparent ages were carried out as described in McDougall and Harrison (1999) using conventional decay constants and isotopic abundances. A summary of $^{40}Ar/^{39}Ar$ ages is given in Table 1; reported ages are at the 1σ uncertainty level.

U-Pb Methods

One volcanic sample [MS-99–4-18-(1)] from the Nangqian basin was dated using the UCLA CAMECA IMS 1270 ion microprobe. The zircons were mounted with a standard in epoxy, polished to 0.25 μm with diamond paste, and coated with 100 Å of Au for analysis. Analyses utilized a 4–8 nA primary O^- beam focused to an ~20 μm spot. Of the mounted zircon grains, three were analyzed. A single U-Pb age was determined by comparison with a working curve defined by measurement of zircon standard AS-3, which yields concordant $^{206}Pb/^{238}U$ and $^{207}Pb/^{235}U$ ages of 1099.1 ± 0.5 Ma by the U-Pb conventional method (Paces and Miller, 1993). Additional details of analytical procedures can be found in Quidelleur et al. (1997) and Dalrymple et al. (1999).

Results

Xialaxiu Volcanics

A rhyolite and a small granitic body found within the Xialaxiu volcanic sequence were sampled for analysis (Fig. 4). Another rhyolite sample was collected from an isolated volcanic flow that unconformably overlies the basal part of the Shanglaxiu basin (Fig. 4). The $^{40}Ar/^{39}Ar$ ages for rhyolite and granitic intrusive within the Xialaxiu volcanic field yield $^{40}Ar/^{39}Ar$ ages of 49.5 ± 0.2 Ma and 49.7 ± 0.2 Ma, respectively, while the isolated rhyolite sample yields a $^{40}Ar/^{39}Ar$ age of 51.2 ± 0.2 Ma (Table 1; Fig. 11). These ages are the same within uncertainty as those obtained by Roger et al. (2000) from the same volcanic field. The age of the Xialaxiu igneous rocks constrain the Shanglaxiu basin and the Shanglaxiu back thrust to predate 51 Ma.

Niuguoda Basin

Two volcanic clasts were collected from a small (800 m × 400 m) outcrop of Paleogene strata unconformably overlying the upper section of the Niuguoda basin fill (Fig. 2). Whole-rock $^{40}Ar/^{39}Ar$ analyses were conducted, owing to a lack of coarse-grained, dateable mineral phases. Both samples yielded identical ages of 101.6 ± 1.3 Ma and 101.6 ± 3.1 Ma (Table 1). These dates provide a lower age boundary for

[2]GSA Data Repository item 2005149, summary of argon isotopic results from the Yushu-Nangqian region, is available on the Web at http://www.geosociety.org/pubs/ft2005.htm. Requests may also be sent to editing@geosociety.org.

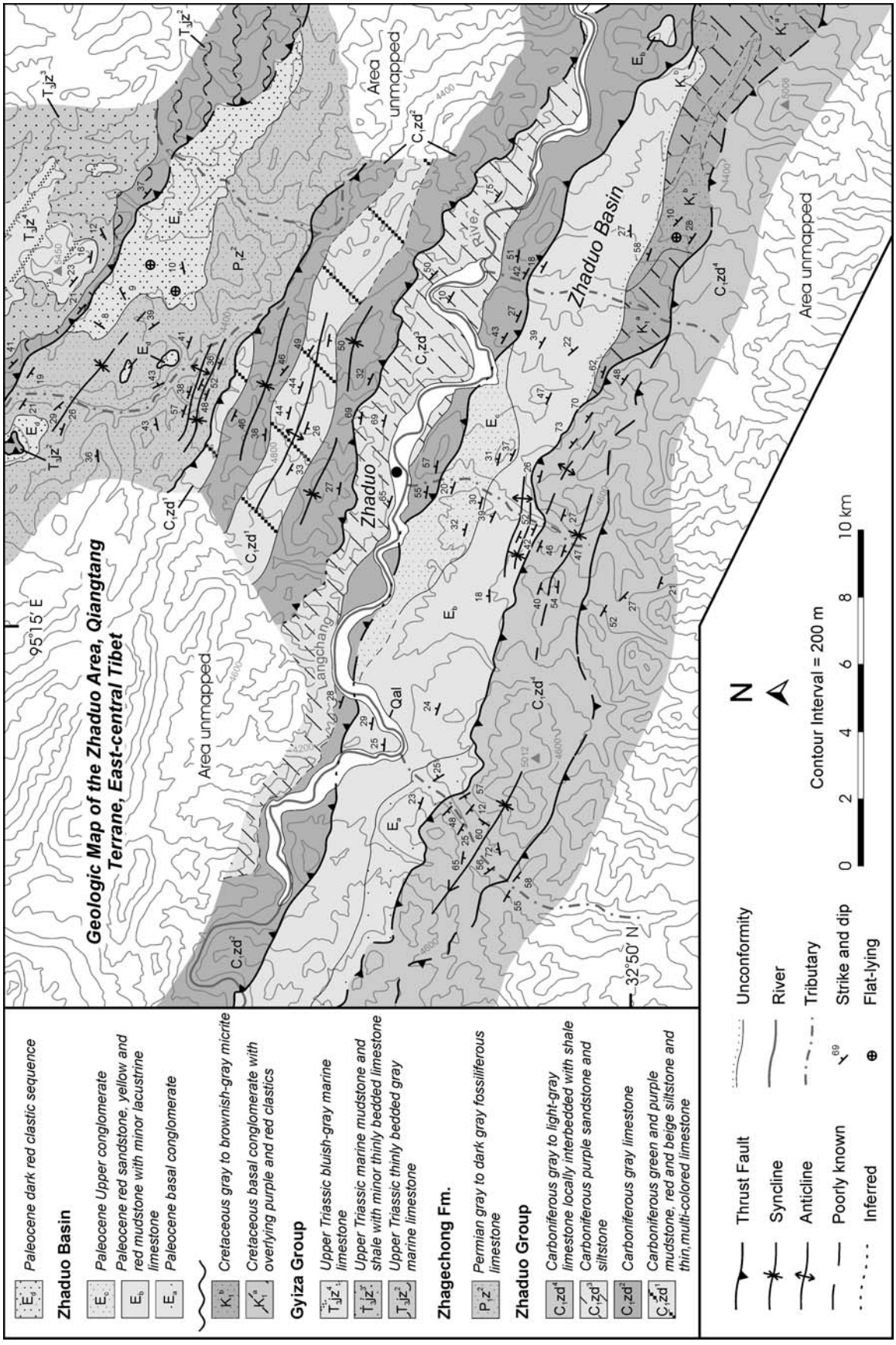

Figure 10. Geologic map of the Zhaduo area.

TABLE 1. SUMMARY OF U-Pb AND $^{40}Ar/^{39}Ar$ AGES FOR IGNEOUS ROCKS IN THE NANGQIAN-YUSHU REGION

Sample	Rock type	Phase	U-Pb age† (Ma)	$^{40}Ar/^{39}Ar$ age‡ (Ma)
Xialaxiu volcanic field				
MS 99–5-12-(1a)	Rhyolite	Biotite	-	49.5 ± 0.2
MS 99–5-12-(2a)	Granite	Biotite	-	49.7 ± 0.2
MS 99–5-10-(1)	Rhyolite	Biotite	-	51.2 ± 0.2
Niuguoda basin				
MS 00–5-8-(1a)	Volcanic clast	Whole rock	-	101.6 ± 0.9
MS 00–5-8-(1b)	Volcanic clast	Whole rock	-	101.6 ± 0.8
Nangqian basin				
MS 00–5-22-(2)	Nepheline-syenite	Biotite	-	37.0 ± 0.2
MS 99–4-27-(1b)	Trachyandesite	Biotite	-	37.2 ± 0.1
MS 99–4-18-(1)	Trachydacite	Zircon, Biotite	36 ± 3.0	37.3 ± 0.2
MS 00–5-9-(2)	Monzonite	Biotite	-	37.3 ± 0.3
MS 00–5-9-(4)	Trachydacite	Biotite	-	37.4 ± 0.1
MS 00–5-25-(1)	Trachydacite	Biotite	-	37.6 ± 0.1
MS 99–4-16-(2)	Basaltic trachyandesite	Biotite	-	37.7 ± 0.2
MS 00–5-9-(3)	Trachydacite	Biotite	-	37.7 ± 0.2
MS 99–4-17-(1)	Monzonite	Biotite	-	37.7 ± 0.2
MS 99–4-15-(3)	Trachyandesite	Biotite	-	37.8 ± 0.1
MS 99–4-28-(1a)	Trachydacite	Biotite	-	38.2 ± 0.1

†Reported weighted mean $^{206}Pb/^{238}U$ age based on comparison with zircon standard AS-3 (1099.1 ± 0.5 Ma; Paces and Miller, 1993); refer to Table 2.
‡Reported ages are weighted means and age uncertainties reflect analytical errors; ages based on comparison with FCT-1 sanidine (27.8 ± 0.3 Ma; McDougall and Harrison, 1999).

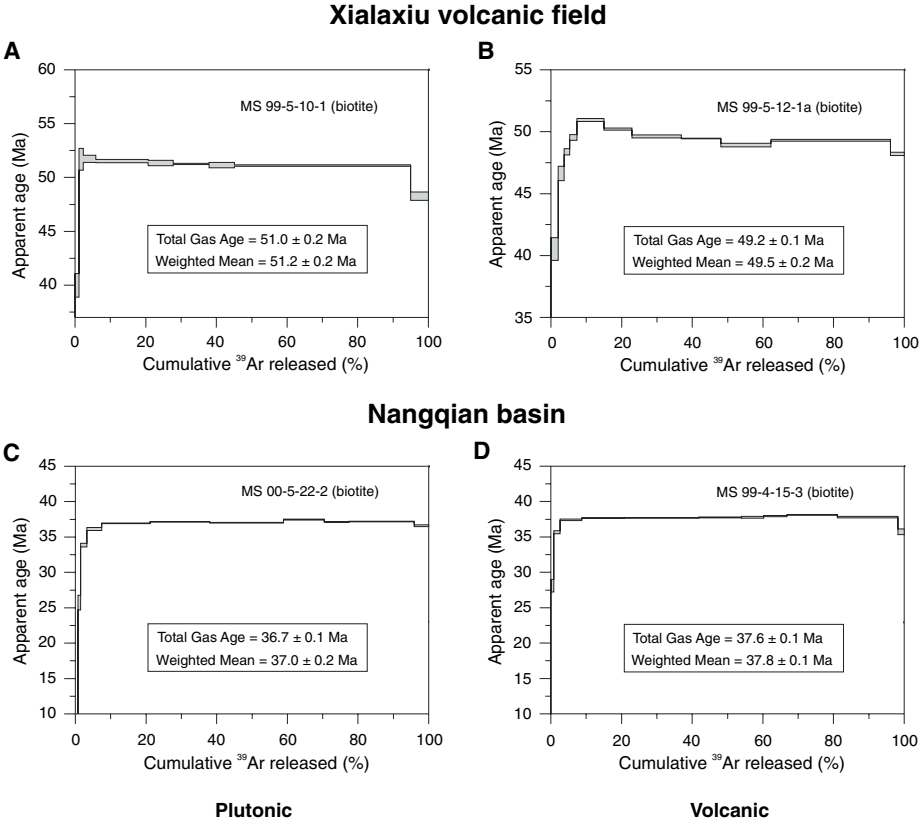

Figure 11. $^{40}Ar/^{39}Ar$ age spectra for selected igneous rocks within (A–B) the Xialaxiu volcanic field and (C–D) the Nangqian basin.

the deposition of the Niuguoda basin. We infer that the 102 Ma clasts were derived from a proximal volcanic source that was produced by subduction of the Indian slab. Cretaceous volcanic rocks in the northern Qiangtang terrane are also reported ~700 km to the west by Yin et al. (1999a) and Kapp (2001).

Nangqian Basin

Eleven samples were collected from igneous rocks in the Nangqian basin (Fig. 6). Eight samples were trachydacite to trachyandesite tuffs and flows are either interbedded with or unconformably overlie the Nangqian basin strata. Another three samples are nepheline-syenite and monzonite hypabyssal intrusions cutting the Nangqian basin sequence. The eight volcanic samples yield $^{40}Ar/^{39}Ar$ ages ranging from 38.2 ± 0.1 Ma to 37.2 ± 0.1 Ma (Table 1). Secondary Ionization Mass Spectrometry (SIMS) analyses for one volcanic sample, dated as 37.3 ± 0.2 Ma by $^{40}Ar/^{39}Ar$, yielded a single U-Pb age of 36 ± 3.0 Ma (Table 2). The three plutonic samples yielded $^{40}Ar/^{39}Ar$ ages ranging from 37.7 ± 0.2 Ma to 37.0 ± 0.2 Ma.

GEOCHEMISTRY

Geochemical Analyses

One sample from the Xialaxiu volcanic field and nine samples from the Nangqian basin dated by $^{40}Ar/^{39}Ar$ and U-Pb methods were analyzed for major and trace element and isotopic compositions from whole-rock analyses (Tables 3 and 4). Major element compositions were determined by wet chemistry, and the trace element data were obtained by inductively coupled plasma–mass spectrometry (ICP-MS) at the Guangzhou Institute of Geochemistry, China.

Results

Xialaxiu Volcanics

A sample from an Eocene rhyolite (49.5 ± 0.2 Ma) was collected from the Xialaxiu volcanic field. The major element geochemistry of the sample indicates that it is calc-alkaline (Table 3). The chondrite-normalized rare earth element (REE) pattern shows a slightly negative Eu anomaly, which may indicate that plagioclase is a major phase involved in fractional crystallization (Fig. 12B). The pattern of normalized trace elements exhibits pronounced negative anomalies in Nb, Ta, Ti, and P, typically indicative of subduction-related magmatism (Fig. 12C) (see discussion by Wang et al., 2001). Our results are broadly similar to those obtained by Roger et al. (2000) for the same

TABLE 2. U-Pb ISOTOPIC DATA

Spot ID[1]	Isotopic ratios							Apparent ages ± 1σ (Ma)		
	$^{206}Pb^*/^{238}U$	±1	$^{207}Pb^*/^{235}U$	±1	$^{207}Pb/^{206}Pb^*$	±1	$^{206}Pb^*$ %	$^{206}Pb^*/^{238}U$	$^{207}Pb^*/^{235}U$	$^{207}Pb^*/^{206}Pb^*$
MS 99–4-18-(1) Nangqian trachydacite										
2,4,1	5.52E-03	6.33E+00	2.54E-02	1.42E+02	3.34E-02	1.39E+02	79.4	35 ± 2	25 ± 36	neg
2,4,2	5.62E-03	8.98E+00	–1.21E-03	–4.76E+03	–1.57E-03	4.76E+03	75.8	36 ± 3	neg	neg
2,9,1	5.64E-03	2.75E+00	1.98E-02	4.60E+01	2.55E-02	4.49E+01	95.9	36 ± 1	20 ± 9	neg
2,9,2	5.61E-03	2.55E+00	1.02E-02	1.25E+02	1.32E-02	1.23E+02	96.6	36 ± 1	10 ± 13	neg
2,9,3	5.07E-03	7.36E+00	2.53E-02	1.73E+02	3.62E-02	1.69E+02	78.0	33 ± 2	25 ± 43	neg
2,9,4	5.88E-03	9.22E+00	4.75E-02	1.14E+02	5.86E-02	1.10E+02	75.4	38 ± 3	47 ± 52	552 ± 2400
2,11,1	5.72E-03	4.06E+00	2.24E-02	8.41E+01	2.84E-02	8.22E+01	92.5	37 ± 2	23 ± 18	neg
2,11,2	5.62E-03	4.12E+00	2.12E-02	7.89E+01	2.73E-02	7.67E+01	95.9	36 ± 1	21 ± 16	neg
2,11,4	6.10E-03	1.03E+01	3.61E-02	1.99E+02	4.29E-02	1.94E+02	67.9	39 ± 4	36 ± 70	neg
2,11,5	5.70E-03	5.75E+00	2.56E-02	1.29E+02	3.26E-02	1.25E+02	85.5	37 ± 2	26 ± 33	neg

[1]Spot identification. #,#,# = row number, grain number, spot number.
*Radiogenic Pb, corrected for common Pb. neg, negative apparent age due to reverse discordance analyses corrected for common Pb using measured ^{204}Pb and Pb evolution models of Stacey and Kramers (1975).

volcanic flows. Given the similar petrology, geochemistry, and age of the Lower Eocene (ca. 51–49 Ma) igneous rocks in the Xialaxiu area, they are most likely cogenetic. These rocks differ geochemically from the younger late middle Eocene (ca. 37 Ma) igneous rocks found in the Nangqian basin to the south; that is, Eocene igneous rocks near Xialaxiu have higher $^{87}Sr/^{86}Sr$ values (~0.7072) and slightly lower $^{143}Nd/^{144}Nd$ values (~0.5125–0.5124) (Roger et al., 2000) (Table 4; Fig. 12A).

Cenozoic high-potassic igneous rocks in northern and eastern Tibet have $^{143}Nd/^{144}Nd$ and $^{87}Sr/^{86}Sr$ isotopic compositions that lie in the enriched extension of the mantle array, but fall far outside the fields of mid-ocean-ridge basalt (MORB), Hawaiian, and Kerguelen basalts (Fig. 12A). The high $^{87}Sr/^{86}Sr$ and low $^{143}Nd/^{144}Nd$ isotope signatures require mantle sources with a time-integrated history of enrichment in light (L) REEs and Rb. A plausible explanation is to ascribe these combined trace-elemental and isotopic observations to a metasomatized subcontinental lithospheric mantle before the onset of partial melting (Arnaud et al., 1992; Turner et al., 1993; Wang et al., 2001). Alternatively, the same geochemical signatures may be explained by partial melting of granulitic or eclogitic Tibetan lower crust (Hacker et al., 2000; Cooper et al., 2002).

Cenozoic igneous rocks in eastern Tibet (western Sichuan) and Yunnan lie along the same Eocene magmatic belt as those we studied in the Yushu-Nangqian area (Roger et al., 2000; Wang et al., 2001). However, the former have lower $^{143}Nd/^{144}Nd$ (<0.5126) and higher $^{87}Sr/^{86}Sr$ (0.7055–0.7070) values compared to the Nangqian volcanics (Zhu et al., 1992; Wang et al., 2001; cf. Fig. 12A). This difference may be explained by the wide age spread of igneous rocks across the region. Igneous rocks with ages of 40–36 Ma are distributed along the entire length of the Ailao Shan–Red River shear zone and its northern extension, the Batang-Lijiang fault system (e.g., Ratschbacher et al., 1996) that links the Yushu-Nangqian thrust belt (Fig. 1) (Leloup et al., 1995; Roger et al., 2000; Wang et al., 2001). The initiation and termination of igneous activity in the Nangqian area occurred at 51 and 37 Ma, which is earlier than along the southern segment of the active Red River fault between 40 and 24 Ma (e.g., Wang et al., 2001 and references therein). Since fractionation of isotopes is a time-dependent process, the lower $^{87}Sr/^{86}Sr$ and higher $^{143}Nd/^{144}Nd$ values of younger igneous rocks in the Red River area to the south (Fig. 12A) may have resulted from continued continental subduction along the eastern margin of the Tibetan Plateau associated with upper crustal shortening as we observed in the Yushu-Nangqian thrust belt. It is possible that the isotopic difference between the Yushu-Nangqian area and the Red River region results from diachronous cessation, from west to east, of Tertiary continental subduction.

Nangqian Basin

Nine of the late middle Eocene igneous samples (37.0 ± 0.2 Ma to 38.2 ± 0.1 Ma) were collected from interbedded volcanic flows in the upper Nangqian basin. The major element geochemistry of the Nangqian volcanic rocks is calc-alkaline, similar to Gangdese plutonic rocks in the southern Lhasa block (Harris et al., 1988) and those studied by Roger et al. (2000) in the Shanglaxiu area and the area to the west in north-central Tibet. Geochemical analyses show enrichment in the major elements (particularly Na and K; Na = 0.98–4.43; K_2O = 7.61–4.12; K_2O/Na_2O = 5.06–1.07), LREEs, and large ion lithophile elements (LILEs; i.e., Rb, Sr, Cs, Ra, etc., see Table 3 and Fig. 12B–C). The patterns of normalized trace elements exhibit pronounced negative anomalies in Nb, Ta, Ti, and P (Fig. 12C), which is a signature of subduction as discussed by Roger et al. (2000) and Wang et al. (2001) for Eocene rocks along the same belt. The content of SiO_2 varies widely in the range of 49.5%–68.5%. We estimate an ~3%–5% volumetric crustal contamination of the Nangqian volcanics, roughly equaling a 90% isotopic contribution by crustal rocks. Isotopic analyses for the high-potassic Nangqian volcanics yield $^{143}Nd/^{144}Nd$ values of ~0.5126 and $^{87}Sr/^{86}Sr$ values that range from 0.7051 to 0.7057 (Table 4).

STRUCTURAL EVOLUTION

Style of Deformation

Because of the lack of involvement of crystalline basement in our mapped areas, we hypothesize that the Cenozoic thrust system is of a thin-skinned style (e.g., Price, 1981) as shown in our cross section (Fig. 3A). This style of deformation is continuous at least for ~90 km west of the Yushu-Nangqian traverse, as demonstrated by our observation in the Zhado area. However, the thin-skinned hypothesis may not be valid laterally to the east of the traverse, because a small gneissic unit occurs within Ordovician strata ~30 km southeast of Yushu (Roger et al., 2003). The gneiss was dated by the U-Pb zircon method that yields a discordia age with a lower intercept at 682 ± 25 Ma and an upper intercept at 2460 ± 74 Ma (Roger et al., 2003). It is possible that a lateral thrust ramp exists east of the Yushu-Nangqian traverse. That is, the basal thrust cuts downsection eastward into the basement east of Yushu exposing the basement rocks. Some 500–700 km to the west of our map area, Kapp et al. (2000, 2003) show that the basement of the central Qiangtang

TABLE 3. GEOCHEMICAL ANALYSES OF MAJOR (%) AND MINOR (PPM) ELEMENTS FOR IGNEOUS ROCKS IN THE NANGQIAN-YUSHU REGION

Sample	MS 00–5-22-(2)	MS 99–4-18-(1)	MS 00–5-9-(2)	MS 00–5-9-(4)	MS 00–5-25-(1)	MS 00–5-9-(3)	MS 99–4-16-(2)	MS 99–4-17-(1)	MS 99–4-15-(3)	MS 99–5-12-(1a)
ICP (%)†										
SiO_2	49.69	63.47	57.71	68.53	64.83	65.47	50.87	67.72	55.36	71.53
Al_2O_3	15.18	16.92	17.27	15.48	16.35	16.53	15.07	15.17	17.85	15.02
Fe_2O_3	4.22	4.55	4.46	1.85	2.81	2.22	4.19	2.11	3.68	1.57
MnO	0.12	0.05	0.09	0.03	0.05	0.06	0.13	0.04	0.10	0.03
MgO	7.59	1.48	3.51	0.53	1.62	1.69	5.39	1.69	3.16	0.95
CaO	10.01	3.17	5.32	1.48	4.00	3.27	14.08	3.26	8.01	2.97
Na_2O	2.43	4.33	4.25	2.96	2.64	4.43	0.98	3.88	1.85	3.07
K_2O	5.90	4.12	4.89	7.61	6.60	4.75	4.95	4.42	7.56	4.13
TiO_2	1.32	0.43	0.98	0.42	0.43	0.44	0.85	0.42	0.59	0.37
P_2O_5	1.23	0.42	0.78	0.32	0.43	0.29	1.18	0.24	0.68	0.23
Total	97.68	98.95	99.25	99.21	99.78	99.16	97.70	98.95	98.83	99.87
ICP-MS (ppm)‡										
Ba	2684	1703	2184	2479	1944	1810	2934	1454	2670	1829
Hf	13.01	6.59	9.35	10.49	7.86	3.95	8.02	5.81	9.05	3.98
Nb	26.89	13.49	26.33	26.25	16.31	14.47	17.85	11.81	19.42	19.94
Pb	31.44	13.12	64.16	58.07	43.55	39.75	76.07	45.32	46.47	30.38
Rb	151.00	115.25	98.51	152.64	128.76	124.91	170.89	94.47	147.48	108.15
Sr	2660	18.05	2391	2185	2215	1728	5003	1152	3186	864
Ta	1.56	0.81	1.54	1.55	0.96	0.88	1.03	0.69	1.11	1.20
Th	35.52	26.82	40.97	39.43	32.33	26.64	42.53	21.65	43.87	25.19
U	7.36	6.28	9.00	9.00	6.80	5.20	8.61	4.94	9.07	5.58
Y	29.20	20.71	27.06	22.76	20.73	18.42	39.54	13.70	31.97	20.97
Zn	103.33	26.69	84.52	57.48	71.20	36.00	92.91	48.09	43.02	24.73
Zr	465.78	240.19	356.90	389.80	297.45	143.93	300.99	215.48	329.56	142.84
La	159.35	104.61	161.87	124.71	127.08	105.56	263.86	70.36	177.95	56.22
Ce	283.97	202.62	290.69	250.76	242.86	196.32	546.32	145.10	345.87	107.94
Pr	35.82	21.56	35.88	27.23	25.70	20.16	67.83	15.88	46.16	10.98
Nd	137.70	78.34	130.42	96.51	91.99	72.00	260.46	58.53	174.85	37.76
Sm	23.30	12.44	20.29	15.88	14.42	11.10	41.68	9.18	29.15	6.54
Eu	5.08	2.69	4.40	3.33	3.04	2.42	8.85	2.12	6.44	1.16
Gd	14.57	8.09	12.01	9.46	8.75	6.86	24.66	5.78	17.19	4.64
Tb	1.59	0.94	1.29	1.04	0.95	0.77	2.45	0.65	1.80	0.70
Dy	6.38	3.98	5.49	4.61	4.06	3.55	9.19	2.75	7.14	3.63
Ho	1.02	0.67	0.91	0.77	0.66	0.55	1.38	0.42	1.03	0.69
Er	2.64	1.82	2.33	2.07	1.79	1.47	3.41	1.11	2.72	1.94
Tm	0.34	0.27	0.32	0.32	0.26	0.21	0.40	0.16	0.34	0.28
Yb	1.96	1.63	2.10	1.79	1.56	1.29	2.54	0.97	2.11	1.87
Lu	0.27	0.25	0.29	0.28	0.22	0.20	0.33	0.16	0.28	0.24
Total (ppm)	673.97	439.90	668.28	538.75	523.34	422.45	1233.36	313.16	813.01	234.59

†Major elements are scaled; FeO omitted.
‡Standards GBPG-1 and AMH-1 used in the analyses. ICP-MS is inductively coupled plasma–mass spectrometry.

TABLE 4. WHOLE ROCK Rb-Sr AND Sm-Nd ISOTOPIC DATA FOR IGNEOUS ROCKS IN THE NANGQIAN-YUSHU REGION

Samples	Age (Ma)	Rb (μg/g)	Sr (μg/g)	$^{87}Rb/^{87}Sr$	$^{87}Sr/^{86}Sr$	±2σ	Sm (μg/g)	Nd (μg/g)	$^{147}Sm/^{144}Nd$	$^{143}Nd/^{144}Nd$	±2σ
MS 00–5-22-(2)	37.0 ± 0.2	100.4	3237	0.08980	0.705090	15	21.66	136.34	0.09598	0.512607	7
MS 99–4-18-(1)	37.3 ± 0.2	110.5	1918	0.1669	0.705662	12	11.97	79.574	0.09098	0.512703	9
MS 00–5-9-(2)	37.3 ± 0.3	93.20	3856	0.07000	0.705300	11	19.26	132.21	0.08812	0.512679	8
MS 00–5-9-(4)	37.4 ± 0.1	218.6	1417	0.4467	0.705156	13	5.894	45.612	0.07816	0.512681	7
MS 00–5-25-(1)	37.6 ± 0.1	205.4	1071	0.5555	0.705458	11	3.519	21.839	0.09747	0.512675	9
MS 00–5-9-(3)	37.7 ± 0.2	142.3	1790	0.2303	0.705248	12	2.740	18.423	0.08996	0.512676	9
MS 99–4-16-(2)	37.7 ± 0.2	90.59	5139	0.05104	0.705390	13	40.78	280.43	0.08796	0.512668	8
MS 99–4-17-(1)	37.7 ± 0.2	133.9	1107	0.3501	0.705100	14	8.603	56.528	0.09206	0.512694	5
MS 99–4-15-(3)	37.8 ± 0.1	126.0	2352	0.1551	0.705305	13	27.18	172.83	0.09513	0.512692	6
MS 99–5-12-(1a)	49.5 ± 0.2	139.1	234.1	1.721	0.707168	12	4.658	31.913	0.08829	0.512543	9

terrane was composed of Triassic blueschist-bearing mélange that may have been subducted from the Songpan-Ganzi terrane beneath the Qiangtang in the latest Triassic. Reflection and refraction seismology indicates that the first-order crustal shortening in the Yushu-Nangqian region is accommodated mainly in the upper crust (Galve et al., 2002). This result is consistent with our assumption that deformation in the Yushu-Nangqian traverse is thin-skinned. Seismic studies by the receiver-function method and the analysis of teleseismic P waves indicate that the Moho is offset along the southern margin of the Qaidam basin, but no offsets are observable along the Jinsha suture and the active left-slip Kunlun fault (Vergne et al., 2002). These observations suggest that if the Paleogene crustal shortening along the Fenghuo Shan–Nangqian thrust belt involves continental subduction, the offset mantle has been "healed," possibly by ductile flow of the lower crust.

Because the detailed structures in the crust along the Yushu-Nangqian traverse are not known, our cross section shown in Figure 3A should be viewed as one of the simplest solutions for downward projection of the observed surface geology. We note that Cenozoic thrusts are widespread in the Qiangtang terrane (Kapp, 2001; Kapp et al., 2005), which is in sharp contrast to the lack of Cenozoic shortening in the Lhasa terrane to the south (e.g., Murphy et al., 1997). This may be due to the fact that basement of the Qiangtang terrane is composed of mechanically much weaker mélange complexes than the crystalline basement of the Lhasa terrane that is most likely similar to the Indian craton as the two were linked in Paleozoic times.

Sequence and Timing of Deformation

Although all major faults are northwest-striking, the Yushu-Nangqian area has experienced multiple episodes of Cenozoic deformation with distinctively different fault kinematics and strain patterns. In the Shanglaxiu area, the Paleogene northeast-directed Shanglaxiu thrust ceased motion by 51 Ma. The thrust together with the overlying Eocene strata was subsequently folded by NE-SW contraction. In the footwall of the Shanglaxiu back thrust, strike-slip faulting postdates NE-SW contraction. Cessation of major Cenozoic thrusts in the Eocene followed by continued NE-SW contraction is also observed along the Xialaxiu and Niuguoda thrusts. In the above area, we could not distinguish whether NE-SW contraction was continuous during and after motion on major thrusts or episodic. However, observations from the Nangqian area strongly suggest that NE-SW contraction occurred in two distinctive phases, between which major phases of strike-slip faulting (both right-slip and left-slip) occurred. Specifically, the Nangqian fault zone has experienced at least five phases of deformation: (1) NE-SW contraction (~60 km) as expressed by northwest-trending folds, minor thrusts, and possible initiation of the main trace of the Fault-B system as an out-of-sequence thrust; (2) right-slip faulting (<3–4 km) coeval or slightly younger than NE-SW contraction, development of the associated en echelon folds, and right-lateral offset of early Eocene basins; (3) development of left-slip faults that terminate into north-trending folds (<3–4 km); (4) renewed NE-SW contraction (>5–10 km) causing folding and thrusting in the Upper Eocene strata; (5) right-slip faulting (< a few km); and (6) active left-slip motion along the Ganzi-Yushu fault (78–100 km, Wang and Burchfiel, 2000).

The youngest phase of NE-SW contraction in the Yushu-Nangqian thrust belt probably occurred during the Neogene, because mapped Neogene strata are deformed by northwest-trending folds and cut by northwest-striking thrusts in the Dongba area. Out-of-sequence thrusting is also evident in the thrust belt as convincingly demonstrated by our mapping in the Zhaduo area where a major Cenozoic thrust locally juxtaposes Triassic strata over Carboniferous and Permian strata.

The north-striking normal fault in the Dongba area is the only extensional structure we mapped in the field. Because it cuts Neogene strata, it must significantly postdate (older than 15–20 Ma) Paleogene igneous activity in the region. However, when east-west extension terminates in the Dongba basin is unclear. The normal fault may have formed synchronously during left-slip faulting along the Ganzi-Yushu fault, similar to structural development of Late Cenozoic rifts and strike-slip faults in central Tibet (Molnar and Tapponnier, 1978; Armijo et al., 1986, 1989; Yin et al., 1999a; Yin, 2000; Taylor et al., 2003). However, the location of the Dongba normal fault is considerably east (>250 km) of the easternmost known rift in Tibet (Armijo et al., 1986, 1989; Taylor et al., 2003).

By integrating the aforementioned crosscutting relationships, we suggest the following deformational history for the Nangqian-Yushu region (Fig. 13): (1) development of the Shanglaxiu (including its back thrust), Xialaxiu, Niuguoda, and Jiangda thrusts and associated folds followed by the initiation of the Nangqian fault zone (the southern branch of the Fault-B system) as an out-of-sequence thrust, (2) development of right-slip faults terminating into east-trending folds and causing development of en echelon folds and right-lateral offset of lower Eocene basin fill, (3) development of left-slip faults that terminate into north-trending folds and reactivate early thrusts and right-slip faults, (4) right-slip faults that cut the Eocene strata overlying the early left-slip faults, (5) renewed NE-SW contraction causing folding of Upper Eocene strata, and (6) development of left-slip and normal faulting.

Regional Correlation

The complex Cenozoic deformational history of the Yushu-Nangqian area is not unique in the eastern Indo-Asian collision zone. Directly south of our study area along the Batang-Lijiang fault zone, Ratschbacher et al. (1996) show the

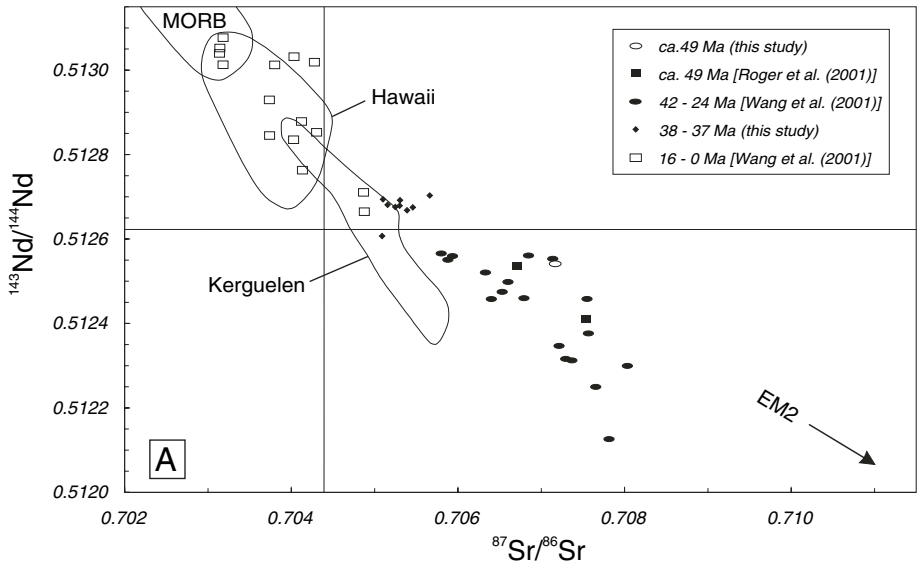

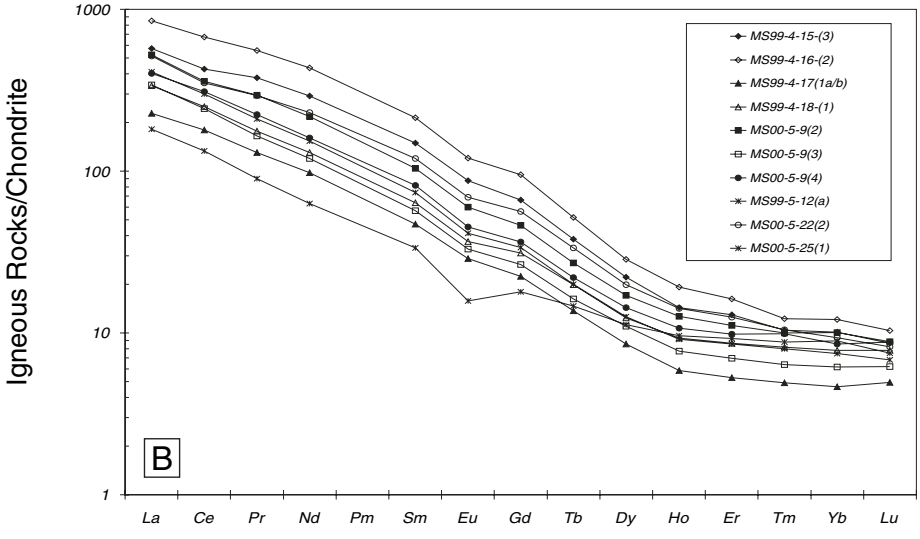

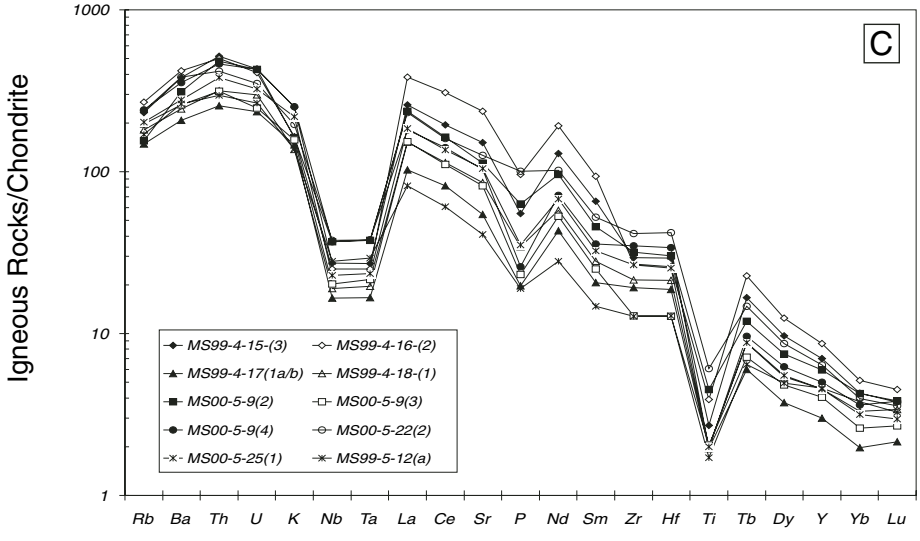

Figure 12. Isotope and trace element data normalized to chondrite values for Cenozoic high-potassic igneous activities. (A) Sr-Nd isotopic diagram. Plotted are Cenozoic volcanic rocks from the Yushu-Nangqian area (Roger et al., 2000; this study) and elsewhere in eastern Tibet and west Yunnan, China (Wang et al., 2001). Fields shown are for mid-ocean-ridge basalt (MORB), Hawaiian, and Kerguelen basalts (Zindler and Hart, 1986) (EM2 enriched mantle end member). (B) Rare earth element (REE) and (C) spider diagrams of trace element data normalized to chondrite values for representative analyses of volcanic rocks of the Yushu-Nangqian area.

region underwent east-west contraction during the Paleogene and early Miocene followed by strike-slip faulting. In the northern Yunnan province of south China ~400 km east of the eastern Himalayan syntaxis and north of the Red River fault, Lacassin et al. (1996) documented activity of a major ductile décollement accommodating SSW-directed thrusting at ca. 36 Ma. This contractional event was followed immediately by the initiation of left-slip motion along the Ailao Shan–Red River shear zone that was coeval with emplacement of leucocratic melts at 22–26 Ma and east-west contraction as expressed by development of the distributed thrust belts on both sides of the left-slip shear zone (Leloup et al., 1995, 2001; Lacassin et al., 1996; Wang and Burchfiel, 1997). The Ailao Shan–Red River shear zone subsequently experienced rapid cooling between 22 and 17 Ma as a result of left-slip transtensional shear (Harrison et al., 1996). Finally, the right-slip Red River fault has reactivated the left-slip Ailao Shan–Red River shear zone since ca. 5 Ma, with coeval north-trending normal faults (Allen et al., 1984; Leloup et al., 1995). The sequence and timing of deformation established by this study match well those along the Ailao Shan–Red River shear zone. That is, both areas experienced Eocene contraction in the NE-SW or NNE-SSW direction, followed first by left-slip faulting and associated east-west contraction and then by right-slip faulting and east-west extension.

The initiation and termination of major faults in the eastern Indo-Asian collision zone are diachronous. For example, the left-slip Wang Chao fault zone in Indochina probably terminated by 30 Ma (Lacassin et al., 1997), significantly older than the termination age of ca. 17 Ma for the Ailao Shan–Red River left-slip shear zone to the north. This northward decrease in fault

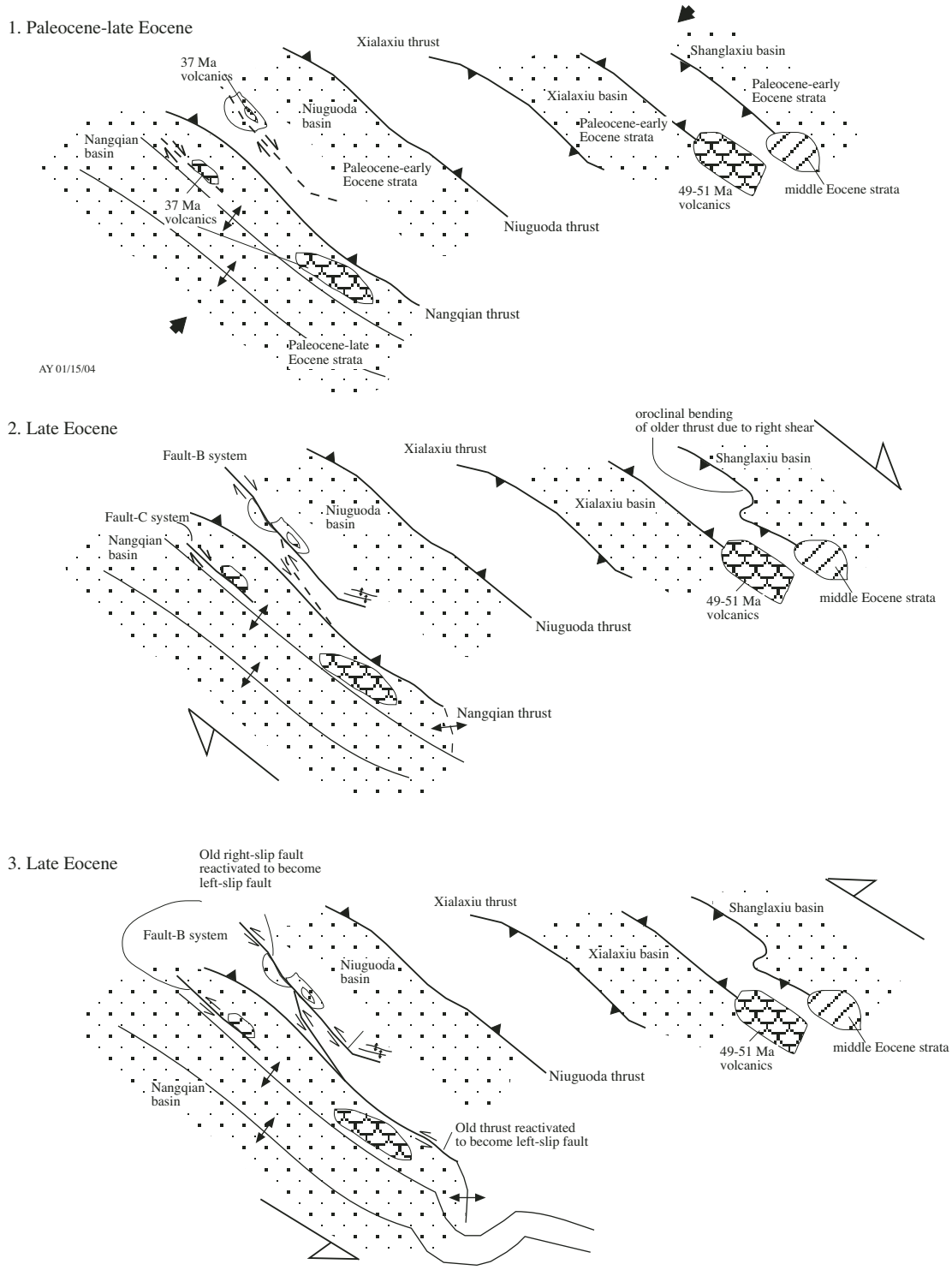

Figure 13. Possible sequence of deformation across the Yushu-Nangqian traverse. (1) NE-SW contraction creating northwest-trending folds and major thrusts and initiation of the Nangqian thrust. (2) Right-slip faulting terminating at east-trending folds and causing development of en echelon folds and right-lateral offset of early Eocene basins. (3) Development of left-slip faults that terminate into north-trending folds. Some of the left-slip faults reactivated early thrusts or right-slip faults. The left-slip faults are overlain by Upper Eocene strata. (4) Development of right-slip faults that offset Upper Eocene strata overlying the left-slip fault zone. (5) Renewed NE-SW contraction causing folding in the Upper Eocene strata. (6) Left-slip and normal faulting. Dashed lines are structures to be developed in the next stage. **(*Continued on following page*.)**

4. Late Eocene

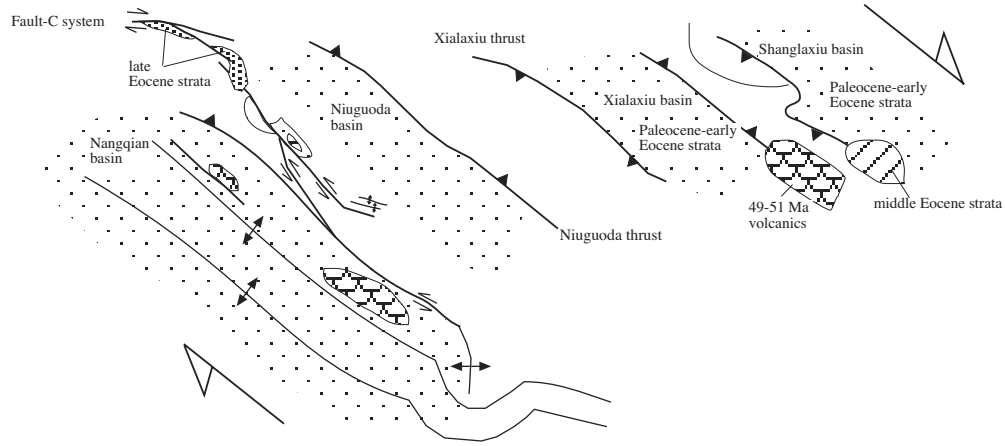

5. Neogene

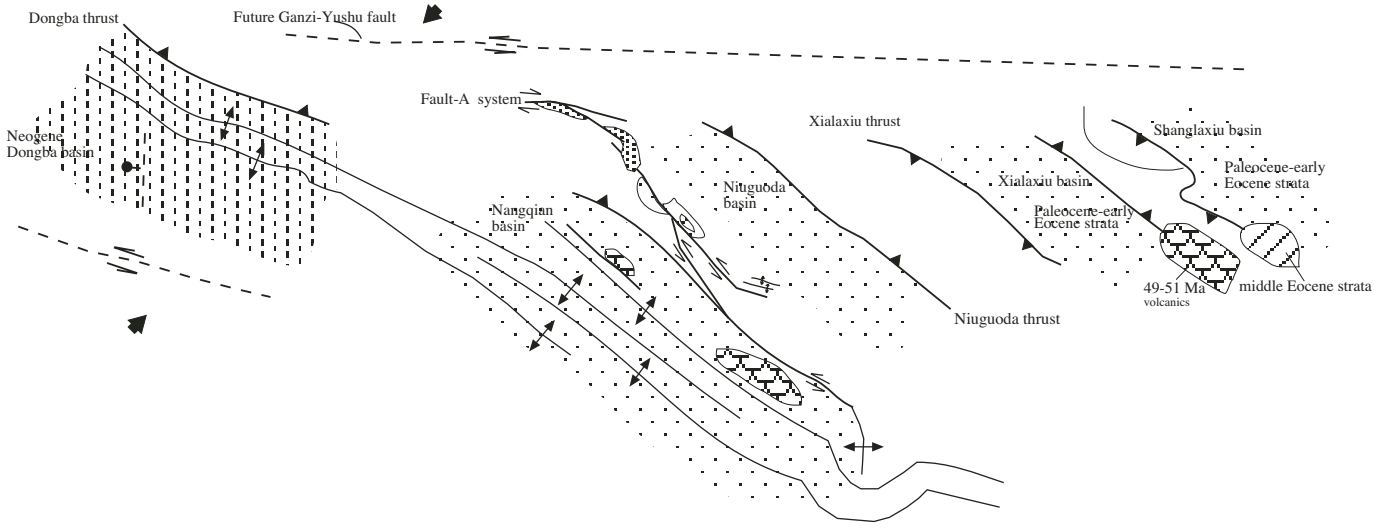

6. Late Neogene-Present

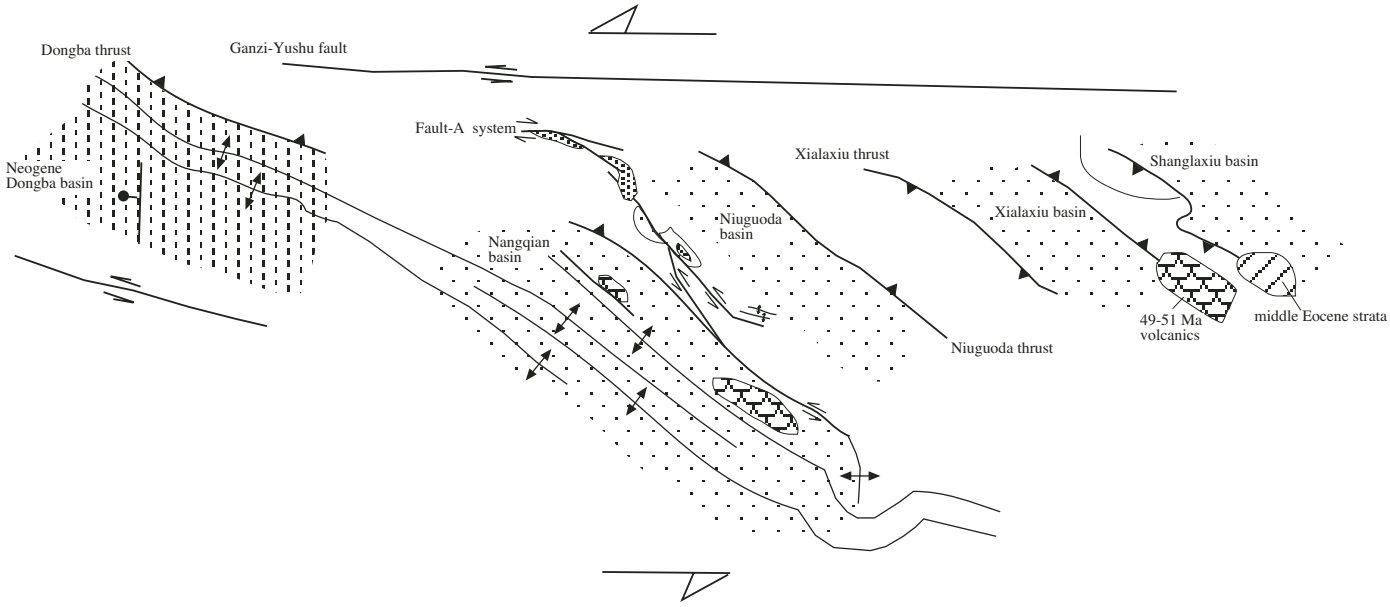

termination age has been related to progressive northward penetration of India into Asia (e.g., Lacassin et al., 1997). However, our observations along the Nangqian fault zone suggest that left-slip faulting postdates the 37 Ma Nangqian volcanics and predates deposition of Upper Eocene strata. That is, although left-slip faulting in the Yushu-Nangqian region could have been initiated coeval with the Ailao Shan–Red River shear zone, its termination is perhaps >15 m.y. older than the latter. The complex evolution of finite-strain fields in the eastern Indo-Asian collision zone has been related to diachronous lateral extrusion of large crustal blocks in the Indo-Asian collisional zone and clockwise rotation around the eastern Himalayan syntaxis (e.g., Peltzer and Tapponnier, 1988; Lacassin et al., 1997; Royden et al., 1997; Wang and Burchfiel, 1997). For complete understanding of regional tectonics and the growth history of the Tibetan Plateau, systematic determination of crustal rotation should be a future research priority so that the observed fault kinematics can be interpreted in the context of the original coordinate systems during the occurrence of each deformational phase.

Relationship between Deformation and Syncollisional Igneous Activity

In the Xialaxiu region, the 49–51 Ma volcanic flows overlie the trace of the Shanglaxiu back thrust. This relationship indicates that the Xialaxiu igneous complex postdates motion along the Shanglaxiu thrust system. Because the Xialaxiu volcanic flows themselves are folded with fold axes trending northwest, NE-SW contraction must have occurred after their emplacement. A critical question is whether the NE-SW contraction was a continuous process before, during, and after the emplacement of the Xialaxiu volcanics and motion on the Shanglaxiu thrust system. As we discussed above, two distinctive phases of NE-SW contraction can be established in the Nangqian area: one in the Paleogene prior to a major strike-slip event and one in the Neogene after the strike-slip event. Therefore, the crosscutting relationship alone in the Xialaxiu area cannot establish whether the volcanic activity was synchronous with contraction. However, based on the Paleocene–early Eocene age of the Xialaxiu basin and its coeval and genetic relationship to thrusts along the basin margin, we know that motion along the Xialaxiu thrusts were active in the Paleocene and early Eocene (Horton et al., 2002), immediately before the deposition of the Xialaxiu volcanics.

In the Nangqian area, the 37 Ma volcanic flows are interlayered with the uppermost part of the Paleocene–late Eocene Nangqian basin fills, which were deposited during NE-SW contractional deformation (Horton et al., 2002). This relationship suggests coeval contraction and magmatic activity in the late Eocene in the Nangqian area. Crosscutting relationships in the Nangqian area also suggest that strike-slip faults postdate the emplacement of the 37 Ma Nangqian igneous complex (Fig. 8). From this and the previous discussion, we conclude that Eocene magmatic activity in the Yushu-Nangqian region occurred during or immediately after a major episode of NE-SW contraction.

Cross Section Restoration

A cross section of the Yushu-Nangqian traverse is shown in Figure 3A. This cross section cannot be strictly balanced because: (1) the presence of late strike-slip faults, (2) some contractional faults may also have strike-slip components (the Fault-B in the Nangqian fault zone), and (3) out-of-sequence thrusting due to either or both pre-Cenozoic folding and multiple phases of Cenozoic shortening creating unusual "younger-over-older" relationships across some of the major contractional faults in this and the Zhaduo areas. The effect of strike-slip faulting on the overall estimate of shortening is probably small, because each fault has slip <2–3 km, based on the offset of Paleogene basins and rapid termination of faults along strike (Fig. 2). In addition, the thrust sheets we mapped are highly deformed. We did not consider the effect of finite strain in cross section construction such as the method proposed by McNaught and Mitra (1996). This is because some of the hanging-wall deformation could be pre-Cenozoic, and an arbitrary choice had to be made to partition the pre-Cenozoic and Cenozoic strain. Thus, in our cross section, internal deformation of the thrust sheets is calculated by first projecting fold geometry downward on the cross section and then measuring the total bed length being shortened. This method implies that all folds in the Shanglaxiu thrust sheet were developed above a décollement zone. Due to the presence of out-of-plane strike-slip faulting, out-of-sequence thrusting, and uncertainties between hanging-wall folds and the underlying basal thrusts, the estimates of crustal shortening provided below are imprecise. Nevertheless, we apply a line-balanced technique wherever possible and believe that our reconstruction captures the first-order geometric and kinematic features of the Yushu-Nangqian fold-thrust belt. Another implicit assumption in our cross section construction is that no subhorizontal shear has occurred at the two ends of the cross section so that pin-lines can be used. Because our section is drawn in the middle of a thrust belt, this assumption may not hold. Therefore, our estimate of total Cenozoic crustal shortening is a minimum amount of shortening for the larger-scale region.

In the northern section, Triassic strata are repeated by imbricate thrusts above an interpreted basal décollement in the T_3jz^1 unit with a depth varying from ~5–8 km (Fig. 3A). In the southern section we use a hanging-wall ramp to explain the occurrence of older Carboniferous strata (Fig. 3A). Thrusting and associated fault-bend and fault-propagation folds north of the Shanglaxiu thrust are related to slip along the basal décollement (Fig. 3A). The basal thrust ramps upsection in the Shanglaxiu thrust footwall from T_3jz^1 sandstone to T_3jz^2 carbonate at the northern end of profile A′–A″ (Fig. 3A).

In the cross section, the Xialaxiu thrust is interpreted to exhibit a hanging-wall flat geometry at the base of T_3jz^1 sandstone (Fig. 3A). Broad folding of the Xialaxiu thrust and the Cenozoic strata in the Xialaxiu basin are attributed to motion on a minor northeast-directed thrust located along the southeastern margin of the basin (Fig. 2). A hanging-wall anticline-syncline pair above the younger thrust is projected in the down-plunge direction beneath the Xialaxiu thrust system (Fig. 3A). Minor, northeast-directed thrusts are present a few kilometers north of the northern margin of the Xialaxiu basin (~4 km south of the Shanglaxiu back thrust) (Fig. 2). Their development may have resulted in the southward tilting of the northern basin margin.

The limited fault slip along the Fault-B system, particularly at its southeastern end, raises the question of why younger Triassic strata are locally placed over older Carboniferous strata. There are at least three explanations: (1) The age assignment of units by Qinghai BGMR (1983a), which we follow in this study, may be wrong. At this point we do not have independent fossil evidence to test this possibility. However, given the fact that Carboniferous strata were deposited in a marine environment, its age identification and regional correlation should be straightforward and we consider an inaccurate age assignment unlikely. (2) There is a major unconformity at the base of Triassic unit T_3jz^2 along which Carboniferous units and older Triassic units have been eroded away. In this scenario northeast-dipping faults in the Fault-B system simply form a fault flat without duplicating or omitting sections. However, as the Carboniferous and even Permian strata are exposed continuous just west of the Nangqian region we mapped (Qinghai BGMR, 1991), we also do not favor this possibility. (3) The Fault-B system is an out-of-sequence structure resulting from two phases of Cenozoic shortening or Cenozoic faulting superposed on pre-Cenozoic folded strata. We favor this explanation because major contractional

A. Stage 1: slip on the Jiangda thrust (JT), Niuguoda thrust (NGT), Niuguoda imbricate thrusts, Shanglaxiu back thrust (SBT) and a north-directed thrust (immediately north of the present Shanglaxiu basin (SB)); deposition of lower Xialaxiu basin (XB), lower Shanglaxiu basin, and lower Niuguoda basin (NDB); erosional denudation of uplifted Permian-Triassic strata to the south (Note: a pre-existing unconformity between Permian strata and underlying Paleozoic strata restores to regional dip).

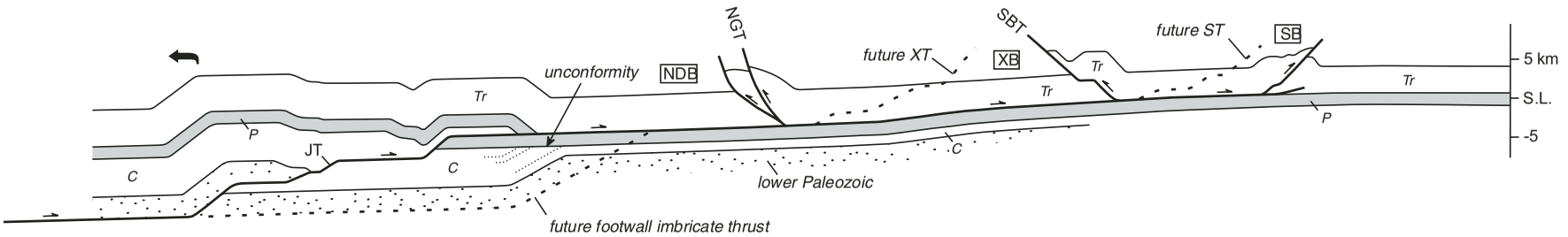

B. Stage 2: folding of the Jiangda thrust by footwall imbrication of pre-Carboniferous-Triassic strata; slip on the Xialaxiu thrust (XT), Xialaxiu imbricate thrust, and Shanglaxiu thrust (ST); deposition of lower to middle Shanglaxiu basin, upper Xialaxiu basin, upper Nuiguoda basin, and lower Nangqian basin (NB); continued slip on thrusts north of Shanglaxiu thrust; continued hinterland erosion of Carboniferous-Triassic strata in the Nangqian area.

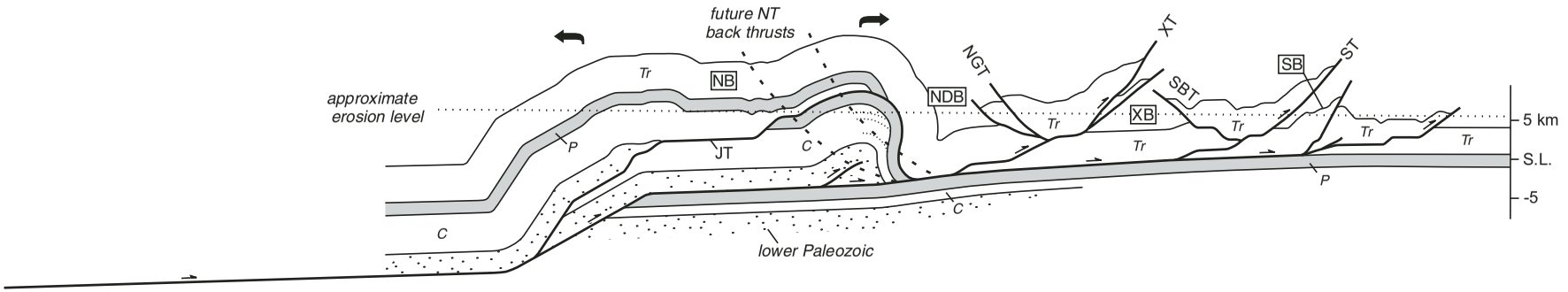

C. Stage 3: minor north-directed thrusting beneath the Xialaxiu thrust; thrusting on the Nangqian thrust (NT) and footwall imbricate thrusts coeval with deposition of middle to upper Nangqian basin; folding of Carboniferous strata in the Nangqian area by minor north- and south-directed thrusting.

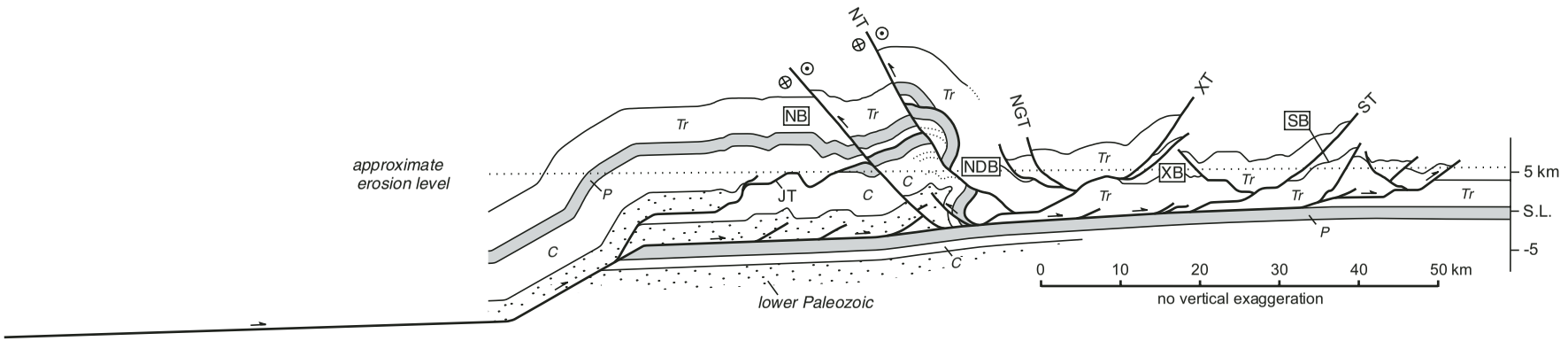

Figure 14. Possible sequence of contractional deformation across the Yushu-Nangqian traverse. S.L.—sea level.

deformation occurred in the Paleocene–early Eocene as expressed by 49–51 Ma volcanic flows overlying the Shanglaxiu fault (Figs. 2 and 4). This occurred prior to motion along the Fault-B system, which must postdate 37 Ma as it cuts the 37–38 Ma Nangqian igneous complex (Figs. 2 and 8). This interpretation is used to show the relationship between the Nangqian thrust and the underlying Permian-Triassic units (Fig. 3A). The overturned fold in the footwall of the Fault-B system at its southeastern end is also projected beneath the Nangqian thrust.

Our interpretation that the folded thrust window 15 km west of Nangqian is part of the Jiangda thrust requires its slip to be at least 6 km (Fig. 2). When restoring the folded fault and displaced Carboniferous units, a minimum of 14–15 km can be inferred for the Jiangda thrust. Folding of the Jiangda thrust may have been related to the development of a minor north-directed blind thrust within Carboniferous strata at a lower structural level (Fig. 3A).

Restoring the cross section shown in Figure 3A requires a minimum of ~43% shortening, that is, ~61 km of shortening across the 83-km-long profile A′–A″. Minimum-slip estimates for individual thrusts from the restored section range from ~2 to 18 km (Fig. 3B). The Yushu-Nangqian thrust belt appears to extend farther to the southeast for another 60 km, based on the presence of Tertiary sedimentary basins shown on regional geologic maps (Qinghai BGMR, 1991). If we extrapolate the estimated 43% shortening from our traverse to the entire width of the ~150-km-wide Yushu-Nangqian fold-thrust belt, our minimum estimated Cenozoic shortening across the northern half of the Qiangtang terrane along the longitude 96°30′°E is roughly 110 km.

A possible sequence of contractional deformation in our map area is shown schematically in Figure 14. In stage 1, the Jiangda thrust initiated as a footwall ramp and feeds slip to a flat along the interface between Triassic and Permian strata (Fig. 14A). As a result, the Niuguoda and Shanglaxiu thrusts were developed above the thrust flat. For clarity we did not show the broad pre-Cenozoic folds. A possible angular unconformity between Permian strata, not exposed in the study area, and the underlying Carboniferous units is also shown below the southern segment of the thrust flat. This assumption helps explain the magnitude and tightness of the inferred large overturned ramp anticline of the Carboniferous units in the Nangqian region (Figs. 2 and 3A). In stage 2, the Xialaxiu thrust was initiated as a footwall thrust splay that cut upsection to merge with the thrust flat along the Permian-Triassic interface (Fig. 14B). Motion across the Xialaxiu thrust ramp further amplified the amplitude of the hanging-wall ramp anticline and may have triggered the development of the Nangqian transpressional system (Fault-B system) as a back thrust across this ramp. The first two stages of fault development occurred during deposition of the Paleocene-Eocene basins exposed along our traverse. In stage 3 (younger than 37 Ma), contraction across the Nangqian fault zone remained active (Fig. 14C).

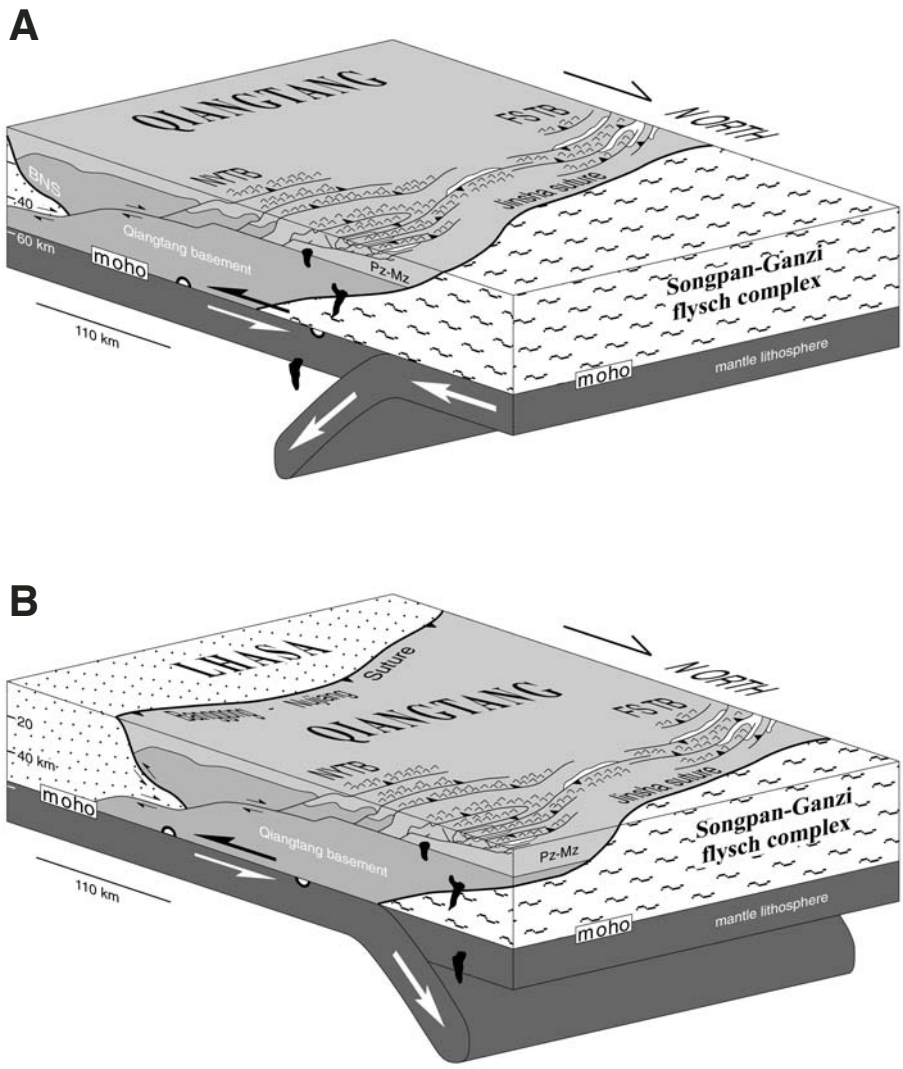

Figure 15. Alternative block models for subduction of mantle lithosphere beneath Qiangtang during Paleogene crustal shortening. (A) Subduction of the Songpan-Ganzi terrane from the north. (B) Subduction of the Lhasa terrane from the south (NYTB—Yushu-Nangqian fold-thrust belt; FSTB—Fenghuo Shan fold-thrust belt; BNS—Banggong-Nujiang suture; Pz-Mz—Paleozoic-Mesozoic strata). (*Continued on following page*.)

MECHANISMS FOR THE FORMATION AND GROWTH OF THE TIBETAN PLATEAU

It has long been known that the Fenghuo Shan thrust belt initiated in the Paleocene and related contraction lasted past the early Miocene (Leeder et al., 1988; Coward et al., 1988; Zhang and Zheng, 1994; Liu and Wang, 2001; Wang et al., 2002; Liu et al., 2003). This study and early work by Horton et al. (2002) expand this temporal framework to the Yushu-Nangqian area. Our results provide new constraints on how the Tibetan Plateau has been uplifted during the Indo-Asian collision.

Our results suggest that >61 km (~45%) Cenozoic shortening was accommodated via thin-skinned thrusting across the 115-km-long Yushu-Nangqian thrust belt. This observation requires that the basement of the Yushu-Nangqian thrust belt be involved with crustal shorten-

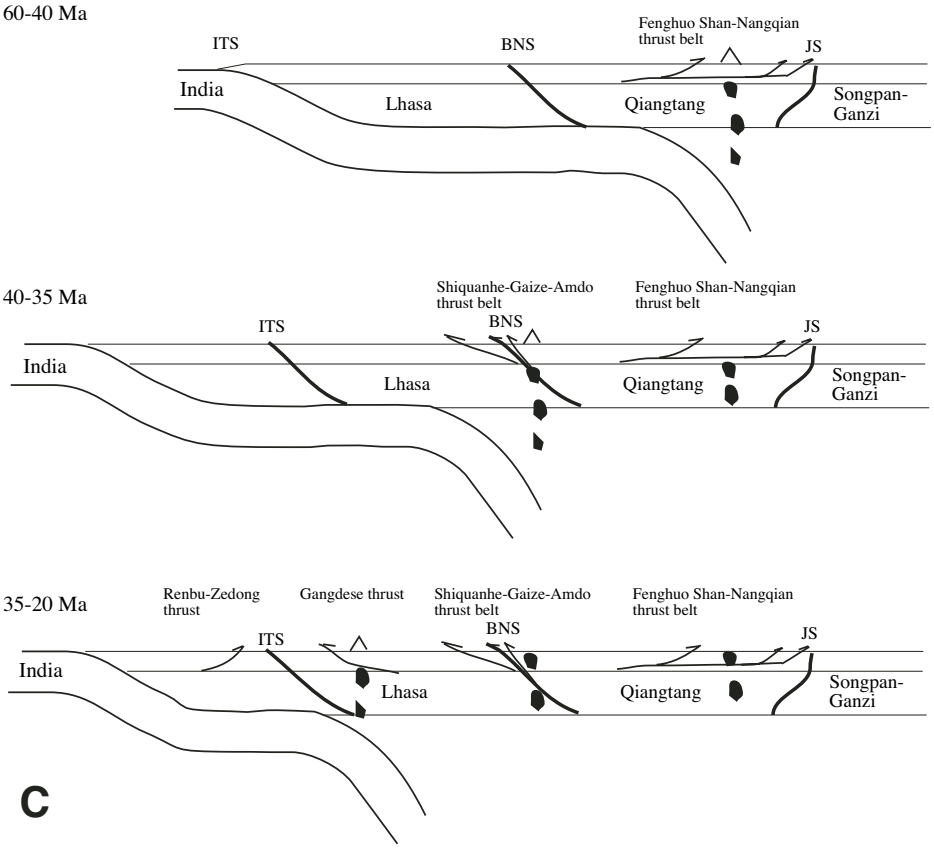

Figure 15 (*continued*). (C) Slab rollback of Indian plate after collision between India and Asia. ITS—Indus Tsangpo suture; JS—Jinsha suture.

ing at depth. We prefer continental subduction as the major accommodation mechanism for the development of the Yushu-Nanqiang thrust belt (Fig. 15A) because it explains (1) coeval development of contraction and magmatism, (2) the geochemical signatures of the Paleogene igneous rocks (also see Wang et al., 2001), and (3) the source of partial melting for the Paleogene magmatism in the mantle lithosphere (e.g., Deng, 1998; Roger et al., 2000; Wang et al., 2001). The continental subduction could be either south-dipping along the Jinsha suture (Tapponnier et al., 2001) or north-dipping along the Banggong-Nujiang suture (Yin and Harrison, 2000; Kapp, 2001; Kapp et al., 2005) (Fig. 15B). It is also possible that rollback of the subducted Indian mantle lithosphere was the cause of syncollisional magmatism in central and southern Tibet (Harrison et al., 2000; DeCelles et al., 2002; Ding et al., 2003) (Fig. 15C). One may also argue that the observed thin-skinned deformation was accommodated by lower crustal flow (e.g., Royden et al., 1997). However, it is not obvious to us how this process could generate partial melting in the mantle lithosphere. It is possible that the lower crustal flow was an important mechanism for plateau uplift in the Neogene. In fact, Royden (1996) showed that lower crustal flow becomes important only some 20 m.y. after initial Indo-Asian collision.

Because syncollisional magmatism occurred over our mapped thin-skinned thrust belt, the inferred continental subduction must have been generated by development of coeval thrust belts outside our study area to the north or south, allowing the basement and underlying mantle lithosphere to be subducted beneath the Yushu-Nangqian traverse. In other words, we do not suggest that thrusting in our study area is the direct cause of the syncollisional magmatism.

It is interesting to note that the initiation of major contractional zones in central and southern Tibet migrated southward, in contrast to the inferred northward progression of deformation in northernmost Tibet (Burchfiel and Royden, 1991; Meyer et al., 1998). Specifically, the Fenghuo Shan–Nangqian thrust belt in central Tibet initiated in the Paleocene-Eocene (Horton et al., 2002; Liu et al., 2003; this study), the Shiquanhe-Gaize-Amdo thrust belt along the Banggong-Nujiang suture zone further south started in the Oligocene (see review by Yin and Harrison, 2000), and the Gangdese thrust along the Indus-Tsangpo suture occurred in the late Oligocene and early Miocene (Yin et al., 1994, 1999b; Harrison et al., 2000). In light of recent results on the chronology of plateau growth in northern Tibet (Yin et al., 2002), it appears that the Tibetan Plateau has grown both northwards and southward from its central part along the oldest Fenghuo Shan–Nangqian thrust belt.

Our study does not support convective removal of Tibetan mantle lithosphere as a major cause for plateau uplift (Molnar et al., 1993), because we observe no coeval extension and syncollisional magmatism in our study area. However, this does not preclude the convective-removal process operating in other parts of Tibet (e.g., Turner et al., 1993). Coeval Paleogene-Eocene contraction and magmatism in the Yushu-Nangqian region is generally consistent with the continental subduction model of Tapponnier et al. (2001) (also see Deng, 1989; Roger et al. 2000; Wang et al., 2001). However, our observations do not support coupled continental subduction and lateral extrusion envisioned by Tapponnier et al. (2001); Paleocene-Eocene contraction is distinctly different from the subsequent left-slip faulting event. In addition, our documented late Eocene right-slip deformation is in contradiction with the predicted left-slip faulting at this time. Finally, our observed Neogene contraction involving major thrusts and intense folding (e.g., in the Dongba area) suggests that significant contraction continued in the Neogene instead of reaching completion in the Eocene as suggested by Tapponnier et al. (2001).

CONCLUSIONS

A complex sequence of Cenozoic deformation occurred across the Yushu-Nangqian fold-thrust belt that has accommodated a minimum of 61 km NE-SW crustal shortening. Cenozoic contraction started prior to 50 Ma and was followed by northwest-striking right-slip and left-slip faults; their motion was brief (probably <3 m.y.) postdating 37 Ma but predating the end of the Eocene. Renewed NE-SW contraction occurred in the Neogene and was later replaced by right-slip faulting. The youngest phase of deformation in the region is east-striking left-slip faulting and associated east-west extension. Our $^{40}Ar/^{39}Ar$ and U-Pb dating of volcanic and plutonic rocks in the study area yields magmatism at 51–49 and 38–37 Ma. The Paleogene magmatism clearly predates Neogene east-west extension, casting doubts on the proposed link between Tibetan extension and syncollisional magmatism. Geochemical analysis supports an interpretation that the igneous rocks were generated by continental subduction. When placing

our results in the regional context, it appears that Cenozoic contractional deformation propagates northward north of Qaidam basin but southward in central and southern Tibet.

ACKNOWLEDGMENTS

Discussions with Paul Kapp and Mike Taylor improved our understanding of Cenozoic deformation and igneous activities in central Tibet. We thank T. Mark Harrison and Marty Grove for their insights and advice regarding $^{40}Ar/^{39}Ar$ and U-Pb analyses. This work was supported by National Science Foundation (NSF) grants EAR-0106677 and EAR-0337191, and a NSF graduate research fellowship. Fault kinematic data were plotted by STEREONET v. 6.3 X by R.W. Allmendinger. Critical reviews by Paul Tapponnier, Peter Molnar, Gerhard Wiesmayr, Mike Edwards, Clark Burchfiel, Richard Law, Lothar Ratschbacher and an anonymous reviewer have significantly improved the original draft of the manuscript.

REFERENCES CITED

Allen, C.R., Gillespie, A.R., Han, Y., Sieh, K.E., Zhang, B., and Zhu, C., 1984, Red River and associated faults, Yunnan province, China: Quaternary geology, slip rates, and seismic hazard: Geological Society of America Bulletin, v. 95, p. 686–700.

Allen, C.R., Luo, Z., Qian, H., Wen, X., Zhou, H., and Huang, W., 1991, Field study of a highly active fault zone: The Xianshuihe fault of southwestern China: Geological Society of America Bulletin, v. 103, p. 1178–1199.

Argand, E., 1924, La tectonique de l'Asie, *in* Proceedings of the Thirteenth International Geologic Congress, p. 170–372.

Armijo, R., Tapponnier, P., Mercier, J.L., and Han, T.-L., 1986, Quaternary extension in southern Tibet: Field observations and tectonic implications: Journal of Geophysical Research, v. 91, p. 13,803–13,872.

Armijo, R., Tapponnier, P., and Han, T., 1989, Late Cenozoic right-lateral strike-slip faulting in southern Tibet: Journal of Geophysical Research, v. 94, p. 2787–2838.

Arnaud, N.O., Vidal, Ph., Tapponnier, P., Matte, P., and Deng, W.M., 1992, The high K_2O volcanism of northwestern Tibet: Geochemistry and tectonic implications: Earth and Planetary Science Letters, v. 111, p. 351–367.

Arne, D., Worley, B., Wilson, C., Chen, S.F., Foster, D., Luo, Z.L., Liu, S.G., and Dirks, P., 1997, Differential exhumation in response to episodic thrusting along the eastern margin of the Tibetan Plateau: Tectonophysics, v. 280, p. 239–256.

Beaumont, C., Jamieson, R.A., Nguyen, M.H., and Lee, B., 2001, Himalayan tectonics explained by extrusion of a low-viscosity crustal channel coupled to focused surface denudation: Nature, v. 414, p. 738–742.

Beck, R.A., Burbank, D.W., Sercombe, W.J., Riley, G.W., Barndt, J.K., Berry, J.R., Afzal, J., Khan, A.M., Jurgen, H., Metje, J., Cheema, A., Shafique, N.A., Lawrence, R.D., and Khan, M.A., 1995, Stratigraphic evidence for an early collision between northwest India and Asia: Nature, v. 373, p. 55–58.

Besse, J., Courtillot, V., Possi, J.P., Westphal, M., and Zhou, Y.X., 1984, Paleomagnetic estimates of crustal shortening in the Himalayan thrusts and Zangbo suture: Nature, v. 311, p. 621–626.

Burchfiel, B.C., and Royden, L.H., 1991, Tectonics of Asia 50 years after the death of Emile Argand: Ecologae Geologicae Helvetiae, v. 84, p. 599–629.

Chung, S.L., Lo, C.C., Lee, T.Y., Zhang, Y., Xie, Y., Li, X., Wang, K.-L., and Wang, P.L., 1998, Diachronous uplift of the Tibetan Plateau starting 40 Myr ago: Nature, v. 394, p. 769–773.

Cooper, K.M., Reid, M.R., Dunbar, N.W., and McIntosh, W.C., 2002, Origin of mafic magmas beneath northwestern Tibet: Constraints from Th-230-U-238 disequilibria: Geochemistry, Geophysics, Geosystems, v. 3, 1065.

Coward, M.P., Butler, R.W.H., Chambers, A.F., Graham, R.H., Izatt, C.N., Khan, M.A., Knipe, R.J., Prior, D.J., Treloar, P.J., and Williams, M.P., 1988, Folding and imbrication of the Indian crust during Himalayan collision: Philosophical Transactions of Royal Society of London, ser. A, v. A326, p. 89–116.

Dalrymple, G.B., Grove, M., Lovera, O.M., Harrison, T.M., Hulen, J.B., and Lanphere, M.A., 1999, Age and thermal history of the Geysers Plutonic Complex (Felsite Unit), Geysers Geothermal Field, California: Earth and Planetary Science Letters, v. 173, p. 285–298.

DeCelles, P.G., Robinson, D.M., and Zandt, G., 2002, Implications of shortening in the Himalayan fold-thrust belt for uplift of the Tibetan Plateau: Tectonics, v. 21, no. 6, 1062.

Deng, W., 1989, Cenozoic volcanic rocks in the northern Ngari district of the Tibet—Discussion on the concurrent subduction: Acta Petrologica Sinica, v. 3, p. 1–11.

Deng, W., 1998, Cenozoic intraplate volcanic rocks in the Northern Qinghai-Xizang Plateau: Beijing, Geologic Publishing House (in Chinese with English abstract), 129 p.

Dewey, J.F., and Burke, K., 1973, Tibetan, Variscan and Precambrian basement reactivation: Products of continental collision: Journal of Geology, v. 81, p. 683–692.

Dewey, J.F., Shackelton, R.M., Chang, C., and Sun, Y., 1988, The tectonic evolution of the Tibetan Plateau: Philosophical Transactions of Royal Society of London, ser. A, v. A326, p. 379–413.

Dewey, J.F., Cande, S., and Pitman, W.C., 1989, Tectonic evolution of the India-Eurasia collision zone: Ecologae Geologicae Helvetiae, v. 82, p. 717–734.

Ding, G., 1984, Active faults of China, *in* A collection of papers of the international symposium on continental seismicity and earthquake prediction: Beijing, China, Seismological Press, p. 225–242.

Ding, L., Kapp, P., Zhong, D.L., and Deng, W.M., 2003, Cenozoic volcanism in Tibet: Evidence for a transition from oceanic to continental subduction: Journal of Petrology, v. 44, p. 1833–1865.

England, P., and Houseman, G., 1986, Finite strain calculations of continental deformation 2. Comparison with the India-Asia collision zone: Journal of Geophysical Research, v. 91, p. 3664–3676.

England, P., and Houseman, G., 1989, Extension during continental convergence, with application to the Tibetan Plateau: Journal of Geophysical Research, v. 94, p. 17,561–17,569.

England, P., and Searle, M., 1986, The Cretaceous-Tertiary deformation of the Lhasa block and implications for crustal thickening in Tibet: Tectonics, v. 5, p. 1–14.

Galve, A., Hirn, A., Mei, J., Gallart, J., de Voogd, B., Lépine, J.C., Diaz, J., Youxue, W., and Hui, Q., 2002, Modes of raising northeastern Tibet probed by explosion seismology: Earth and Planetary Science Letters, v. 203, p. 35–43.

Hacker, B.R., Gnos, E., Ratschbacher, L., Grove, M., McWilliams, M., Sobolev, S.V., Wan, J., and Wu, Z.H., 2000, Hot and dry deep crustal xenoliths from Tibet: Science, v. 287, p. 2463–2466.

Harris, N.B.W., Xu, R., Lewis, C.L., Hawkesworth, C.J., and Zhang, Y., 1988, Isotope geochemistry of the 1985 Tibet Geotraverse, Lhasa to Golmud: Philosophical Transactions of the Royal Society of London, ser. A, v. A237, p. 263–285.

Harrison, T.M., Copeland, P., Kidd, W.S.F., and Yin, A., 1992, Raising Tibet: Science, v. 255, p. 1663–1670.

Harrison, T.M., Leloup, P.H., Ryerson, F.J., Tapponnier, P., Lacassin, R., and Chen, W., 1996, Diachronous initiation of transtension along the Ailao Shan–Red River shear zone, Yunnan and Vietnam, *in* Yin, A., and Harrison, T.M., eds., The tectonic evolution of Asia: New York, Cambridge University Press, p. 208–226.

Harrison, T.M., Yin, A., Grove, M., Lovera, O.M., and Ryerson, F.J., 2000, The Zedong window: A record of superposed Tertiary convergence in southeastern Tibet: Journal of Geophysical Research, v. 105, p. 19,211–19,230.

Hildebrand, P.R., Noble, S.R., Searle, M.P., Waters, D.J., and Parrish, R.R., 2001, Old origin for an active mountain range: Geology and geochronology of the eastern Hindu Kush, Pakistan: Geological Society of America Bulletin, v. 113, p. 625–639.

Horton, B.K., Yin, A., Spurlin, M.S., Zhou, J., and Wang, J., 2002, Paleocene-Eocene syncontractional sedimentation in narrow, lacustrine-dominated basins of east-central Tibet: Geological Society of America Bulletin, v. 114, p. 771–786.

Kapp, P.A., 2001, Tectonic evolution of the Qiangtang terrane and Banggong-Nujiang suture zone, central Tibet [Ph.D. thesis]: Los Angeles, University of California, 285 p.

Kapp, P.A., Yin, A., Manning, C.E., and Murphy, M.A., Harrison, T.M., Spurlin, M., Ding, L., Deng, X., and Wu, C.M., 2000, Blueschist-bearing metamorphic core complexes in the Qiangtang block reveal deep crustal structure of northern Tibet: Geology, v. 28, p. 19–22.

Kapp, P., Yin, A., Manning, C.E., Harrison, T.M., Taylor, M.H., and Ding, L., 2003, Tectonic evolution of the early Mesozoic blueschist-bearing Qiangtang metamorphic belt, central Tibet: Tectonics, v. 22, no. 4, p. 1043.

Kapp, P., Yin, A., Harrison, T.M., Ding, L., Deng, X.G., and Zhou, Y., 2005, Cretaceous-Tertiary shortening, basin development, and volcanism in central Tibet: Geological Society of America Bulletin, v. 117, p. 865–878.

Klootwijk, C.T., Gee, F.S., Peirce, J.W., Smith, G.M., and McFadden, P.L., 1992, An early India contact: Paleomagnetic constraints from Ninetyeast Ridge, ODP Leg 121: Geology, v. 20, p. 395–398.

Klootwijk, C.T., Conaghan, P.J., Nazirullah, R., and de Jong, K.A., 1994, Further palaeomagnetic data from Chitral (Eastern Hindukush): Evidence for an early India-Asia contact: Tectonophysics, v. 237, p. 1–25.

Lacassin, R., Scharer, U., Leloup, P.H., Arnaud, N., Tapponnier, P., Liu, X.H., and Zhang, L.S., 1996, Tertiary deformation and metamorphism SE of Tibet: The folded tiger-leap décollement of NW Yunnan, China: Tectonics, v. 15, p. 605–679.

Lacassin, R., Maluski, H., Leloup, P.H., Tapponnier, P., Hinthong, C., Siribhakdi, K., Chuaviroj, S., and Charoenravat, A., 1997, Tertiary diachronic extrusion and deformation of western Indochina: Structural and Ar-40/Ar-39 evidence from NW Thailand: Journal of Geophysical Research, v. 102, p. 10,013–10,037.

Leeder, M.R., Smith, A.B., and Yin, J., 1988, Sedimentology, palaeoecology and palaeoenvironmental evolution of the 1985 Lhasa to Golmud Geotraverse: Philosophical Transactions of the Royal Society of London, ser. A, v. 327, p. 107–143.

Leloup, P.H., Lacassin, R., Tapponnier, P., Scharer, U., Zhong, D.L., Liu, X.H., Zhang, L.S., Ji, S.C., and Trinh, P.T., 1995, The Ailao Shan–Red River shear zone (Yunnan, China), Tertiary transform boundary of Indochina: Tectonophysics, v. 251, p. 3–84.

Leloup, P.H., Arnaud, N., Lacassin, R., Kienast, J.R., Harrison, T.M., Trong, T.T.P., Replumaz, A., and Tapponnier, P., 2001, New constraints on the structure, thermochronology, and timing of the Ailao Shan–Red River shear zone, SE Asia: Journal of Geophysical Research, v. 106, p. 6683–6732.

Le Pichon, X., Fournier, M., and Jolivet, L., 1992, Kinematics, topography, shortening, and extrusion in the India-Asian collision: Tectonics, v. 11, p. 1085–1098.

Liu, Z.Q., 1988, Geologic map of the Qinghai-Xizang Plateau and its neighboring regions: Beijing, Chengdu Institute of Geology and Mineral Resources, Geologic Publishing House, scale 1:1,500,000.

Liu, Z., and Wang, C., 2001, Facies analysis and depositional systems of Cenozoic sediments in the Hoh Xil basin, northern Tibet: Sedimentary Geology, v. 140, p. 251–270.

Liu, Z.F., Zhao, X.X., Wang, C.S., Liu, S., and Yi, H.S., 2003, Magnetostratigraphy of Tertiary sediments from the Hoh Xil basin: Implications for the Cenozoic tectonic history of the Tibetan Plateau: Geophysical Journal International, v. 154, p. 233–252.

Lovera, O.M., Grove, M., Harrison, T.M., and Mahon, K.I., 1997, Systematic analysis of K-feldspar $^{40}Ar/^{39}Ar$ step-heating experiments: Significance of activation energy determinations: Geochimica et Cosmochimica Acta, v. 61, p. 3171–3192.

Mattauer, M., 1986, Intracontinental subduction, crustal stacking wedge and crust-mantle decollement, *in* Coward, M.P., and Ries, A.C., eds., Collision Tectonics: Geological Society [London] Special Publication 19, p. 37–50.

McDougall, I., and Harrison, T.M., 1999, Geochronology and thermochronology by the $^{40}Ar/^{39}Ar$ method: New York, Oxford University Press, 212 p.

McNaught, M., and Mitra, G., 1996, The use of finite strain data in constructing a retrodeformable cross section of the Meade thrust sheet, southeastern Idaho, U.S.A.: Journal of Structural Geology, v. 18, p. 573–583.

Meyer, B., Tapponnier, P., Bourjot, L., Metivier, F., Gaudemer, Y., Peltzer, G., Shunmin, G., and Zhitai, C., 1998, Crustal thickening in Gansu-Qinghai, lithospheric mantle subduction, and oblique, strike-slip controlled growth of the Tibet Plateau: Geophysical Journal International, v. 135, p. 1–47.

Molnar, P., and Tapponnier, P., 1975, Cenozoic tectonics of Asia; effects of a continental collision: Science, v. 189, p. 419–426.

Molnar, P., and Tapponnier, P., 1978, Active tectonics of Tibet: Journal of Geophysical Research, v. 85, p. 5361–5375.

Molnar, P., England, P., and Martinod, J., 1993, Mantle dynamics, the uplift of the Tibetan Plateau, and the Indian monsoon: Review of Geophysics, v. 31, p. 357–396.

Murphy, M.A., Yin, A., Harrison, T.M., Durr, S.B., Chen, Z., Ryerson, F.J., Kidd, W.S.F., Wang, X., and Zhou, X., 1997, Significant crustal shortening in southern Tibet prior to the Indo-Asian collision: Geology, v. 25, p. 719–722.

Ni, J., and Barazangi, M., 1984, Seismotectonics of the Himalayan collision zone: Geometry of the underthrusting Indian plate beneath the Himalaya: Journal of Geophysical Research, v. 89, p. 1147–1163.

Nie, S., Yin, A., Rowley, D., and Jin, Y., 1994, Exhumation of the Dabie Shan ultra-high pressure rocks and accumulation of the Songpan-Ganzi flysch sequence, central China: Geology, v. 22, p. 999–1002.

Owens, T.J., and Zandt, G., 1997, Implications of crustal property variations for models of Tibetan Plateau evolution: Nature, v. 387, p. 37–43.

Pacers, J.B., and Miller, J.D., 1993, The precise U-Pb ages of Duluth complex and related mafic intrusions, northeastern Minnesota—geochronological insights to physical, petrogenic, paleomagnetic, and tectonomagmatic processes associated with the 1.1 Ga midcontinent rift system: Journal of Geophysical Research, v. 98, p. 13,997–14,013.

Pan, G.T., Wang, P.S., Xu, Y.R., Jiao, S.P., and Xiang, T.S., 1990, Cenozoic tectonic evolution of Qinghai-Xizang Plateau: Beijing, Geological Publishing House, 190 p.

Patriat, P., and Achache, J., 1984, India-Eurasia collision chronology has implications for crustal shortening and driving mechanism of plates: Nature, v. 311, p. 615–621.

Peltzer, G., and Tapponnier, P., 1988, Formation and evolution of strike-slip faults, rifts, and basins during the India-Asia collision: An experimental approach: Journal of Geophysical Research, v. 93, p. 15,085–15,117.

Powell, C.M., and Conaghan, P.G., 1973, Plate tectonics and the Himalayas: Earth and Planetary Science Letters, v. 20, p. 1–12.

Price, R., 1981, The Cordilleran foreland thrust and fold belt in southern Canadian Rocky Mountains, *in* McClay, K.R., and Price, N.J., eds., Thrust and nappe tectonics: Geological Society [London] Special Publication 9, p. 427–448.

Qinghai BGMR, (Qinghai Bureau of Geology and Mineral Resources), 1983a, Geologic map of the Nangqian region, with geologic report: unpublished, 198 p., scale 1:200,000.

Qinghai BGMR, (Qinghai Bureau of Geology and Mineral Resources), 1983b, Geologic map of the Shanglaxiu region, with geologic report: unpublished, 220 p., scale 1:200,000.

Qinghai BGMR, (Qinghai Bureau of Geology and Mineral Resources), 1988, Geologic map of the Jiduo region, with geologic report: unpublished, 203 p., scale 1:200,000.

Qinghai BGMR, (Qinghai Bureau of Geology and Mineral Resources), 1991, Regional Geology of Qinghai Province: Beijing, Geological Publishing House, 662 p.

Quidelleur, X., Grove, M., Lovera, O.M., Harrison, T.M., Yin, A., and Ryerson, J.F., 1997, The thermal evolution and slip history of the Renbu Zedong thrust, southeastern Tibet: Journal of Geophysical Research, v. 102, p. 2659–2679.

Ratschbacher, L., Frisch, W., Chen, C., and Pan, G., 1996, Cenozoic deformation, rotation, and stress patterns in eastern Tibet and western Sichuan, China, *in* Yin, A., and Harrison, T.M., eds., The tectonic evolution of Asia: New York, Cambridge University Press, p. 227–249.

Roger, F., Tapponnier, P., Arnaud, N., Schärer, U., Maurice, B., Zhiqin, X., and Jingsui, Y., 2000, An Eocene magmatic belt across central Tibet: Mantle subduction triggered by the Indian collision?: Terra Nova, v. 12, p. 102–108.

Roger, F., Arnaud, N., Gilder, S., Tapponnier, P., Jolivet, M., Brunel, M., Malavieille, J., Xu, Z.Q., and Yang, J.S., 2003, Geochronological and geochemical constraints on Mesozoic suturing in east central Tibet: Tectonics, v. 22, no. 4, 1037.

Rowley, D.B., 1996, Age of collision between India and Asia: A review of the stratigraphic data: Earth and Planetary Science Letters, v. 145, p. 1–13.

Royden, L., 1996, Coupling and decoupling of crust and mantle in convergent orogens: Implications for strain partitioning in the crust: Journal of Geophysical Research, v. 101, p. 17,679–17,705.

Royden, L.H., Burchfiel, B.C., King, R.W., Wang, E., Chen, Z., Shen, F., and Liu, Y., 1997, Surface deformation and lower crustal flow in eastern Tibet: Science, v. 276, p. 788–790.

Şengör, A.M.C., and Natal'in, B.A., 1996, Paleotectonics of Asia: Fragments of a synthesis, *in* Yin, A., and Harrison, T.M., eds., The tectonic evolution of Asia: New York, Cambridge University Press, p. 486–640.

Stacey, J.S., and Kramers, J.D., 1975, Approximation of terrestrial lead isotope evolution by a two-stage model: Earth and Planetary Science Letters, v. 26, p. 207–221.

Tapponnier, P., Lacassin, R., Leloup, P.H., Scharer, U., Zhong, D.L., Wu, H.W., Liu, X.H., Ji, S.C., Zhang, L.S., and Zhong, J.Y., 1990, The Ailao Shan/Red River metamorphic belt Tertiary left-lateral shear between Indochina and South China: Nature, v. 343, p. 431–437.

Tapponnier, P., Xu, Z.Q., Roger, F., Meyer, B., Arnaud, N., Wittlinger, G., and Yang, J.S., 2001, Geology—Oblique stepwise rise and growth of the Tibet Plateau: Science, v. 294, p. 1671–1677.

Taylor, M., Yin, A., Ryerson, F.J., Kapp, P., and Ding, L., 2003, Conjugate strike-slip faulting along the Bangong-Nujiang suture zone accommodates coeval east-west extension and north-south shortening in the interior of the Tibetan Plateau: Tectonics, v. 22, p. 1044.

Turner, S., Hawkesworth, C.J., Liu, J., Rogers, N., Kelley, S., and van Calsteren, P., 1993, Timing of Tibetan uplift constrained by analysis of volcanic rocks: Nature, v. 364, p. 50–53.

Vergne, J., Wittlinger, G., Hui, Q., Tapponnier, P., Poupinet, G., Mei, J., Herquel, G., and Paul, A., 2002, Seismic evidence for stepwise thickening of the crust across the NE Tibetan Plateau: Earth and Planetary Science Letters, v. 203, p. 25–33.

Wang, C.S., Liu, Z.F., Yi, H.S., Liu, S., and Zhao, X.X., 2002, Tertiary crustal shortenings and peneplanation in the Hoh Xil region: Implications for the tectonic history of the northern Tibetan Plateau: Journal of Asian Earth Sciences, v. 20, p. 211–223.

Wang, E., and Burchfiel, B.C., 1997, Interpretation of Cenozoic tectonics in the right-lateral accommodation zone between the Ailao Shan shear zone and the eastern Himalayan syntaxis: International Geological Review, v. 39, p. 191–219.

Wang, E., and Burchfiel, B.C., 2000, Late Cenozoic to Holocene deformation in southwestern Sichuan and adjacent Yunnan, China, and its role in the formation of the southeastern part of the Tibetan Plateau: Geological Society of America Bulletin, v. 112, p. 413–423.

Wang, E., Burchfiel, B.C., Royden, L.H., Liangzhong, C., Jishen, C., Wenxin, L., and Zhiliang, C., 1998, Late Cenozoic Xianshuihe-Xiaojiang, Red River, and Dali fault systems of southwestern Sichuan and central Yunnan, China: Geological Society of America Special Paper 327, 108 p.

Wang, J.H., Yin, A., Harrison, T.M., Grove, M., Zhang, Y.Q., and Xie, G.H., 2001, A tectonic model for Cenozoic igneous activities in the eastern Indo-Asian collision zone: Earth and Planetary Science Letters, v. 188, p. 123–133.

Willett, S.D., and Beaumont, C., 1994, Subduction of Asian lithospheric mantle beneath Tibet inferred from models of continental collision: Nature, v. 369, p. 642–645.

Worley, B., Powell, R., and Wilson, C.J.L., 1997, Crenulation cleavage formation: Evolving diffusion, deformation and equilibration mechanisms with increasing metamorphic grade: Journal of Structural Geology, v. 19, p. 1121–1135.

Xu, G., and Kamp, P.J., 2000, Tectonics and denudation adjacent to the Xianshuihe fault, eastern Tibetan Plateau: Constraints from fission track thermochronology: Journal of Geophysical Research, v. 105, p. 19,231–19,251.

Yin, A., 2000, Mode of Cenozoic east-west extension in Tibet suggesting a common origin of rifts in Asia during the Indo-Asian collision: Journal of Geophysical Research, v. 105, p. 21,745–21,759.

Yin, A., and Harrison, T.M., 2000, Geologic evolution of the Himalayan-Tibetan orogen: Annual Review of Earth and Planetary Sciences, v. 28, p. 211–280.

Yin, A., and Nie, S., 1993, An indentation model for North and South China collision and the development of the Tanlu and Honam fault systems, eastern Asia: Tectonics, v. 12, p. 801–813.

Yin, A., and Nie, S., 1996, A Phanerozoic palinspastic reconstruction of China and its neighboring regions, *in* Yin, A., and Harrison, T.M., eds., The tectonic evolution of Asia: New York, Cambridge University Press, p. 18–35.

Yin, A., Harrison, T.M., Ryerson, F.J., Chen, W., Kidd, W.S.F., and Copeland, P., 1994, Tertiary structural evolution of the Gangdese thrust system in southern Tibet: Journal of Geophysical Research, v. 99, p. 18,175–18,201.

Yin, A., Kapp, P.A., Murphy, M.A., Manning, C.E., Harrison, T.M, Grove, M., Ding, L., Deng, X., and Wu, C.M., 1999a, Evidence for significant late Cenozoic E-W extension in north Tibet: Geology, v. 27, p. 787–790.

Yin, A., Harrison, T.M., Murphy, M.A., Grove, M., Nie, S., Ryerson, F.J., Wang, X., and Chen, Z., 1999b, Tertiary deformation history of southeastern and southwestern Tibet during the Indo-Asian collision: Geologic Society of America Bulletin, v. 111, p. 1644–1664.

Yin, A., Rumelhart, P.E., Butler, R., Cowgill, E., Harrison, T.M., Foster, D.A., Ingersoll, R.V., Zhang, Q., Zhou, X., Wang, X., Hanson, A., and Raza, A., 2002, Tectonic history of the Altyn Tagh fault system in northern Tibet inferred from Cenozoic sedimentation: Geological Society of America Bulletin, v. 114, p. 1257–1295.

Zhang, Y., and Zheng, J., 1994, Geologic overview in Kokshili, Qinghai and adjacent areas: Beijing, Seismological Publishing House, p. 177 (in Chinese with English abstract).

Zhao, W., and Morgan, W.J., 1987, Injection of Indian crust into Tibetan lower crust: A two-dimensional finite element model study: Tectonics, v. 6, p. 489–504.

Zhou, D., and Graham, S.A., 1996, The Songpan-Ganzi complex of the West Qingling Shan as a Triassic remnant ocean basin, *in* Yin, A., and Harrison, T.M., eds., The tectonics of Asia: New York, Cambridge University Press, p. 281–299.

Zhu, B.Q., Zhang, Y.Q., and Xie, Y.W., 1992, Isotope characteristics of Cenozoic potassic volcanic rocks from Haidong, Yunnan, and their implications for subcontinental mantle evolution in southwestern China: Geochimica, v. 21, p. 201–212.

Zindler, A., and Hart, S.R., 1986, Chemical geodynamics: Annual Review of Earth and Planetary Sciences, v. 14, p. 493–571.

Manuscript Received by the Society 23 January 2004
Revised Manuscript Received 22 September 22 2004
Manuscript Accepted 16 November 2004

Printed in the USA